# Modelling lithium-ion battery cost, emissions, material criticality and performance

Model documentation version 2.0 (IN DEVELOPMENT)

Joris Baars
Newcastle University, UK

March 4, 2022

## Contents

## List of Abbreviations

**BOM** Bill of materials

**CAM** Cathode active material

**CMC** Carboxymethyl cellulose

**EPA** Environmental Protection Agency

**HWFET** Highway Fuel Economy Test

**LFP** Lithium iron phosphate

**NCA** Lithium nickel cobalt aluminum oxide

**NMC** Lithium nickel manganese cobalt oxide

**PCPM** Product costs and profit margins

**PET** Polyethylene terephthalate

**PP** Polypropylene

**PVDF** Polyvinylidene fluoride

**SBR** Styrene-Butadiene Rubber

**SOC** State of charge

**UDDS** Urban Dynamometer Driving Schedule

# 1. Supplementary information battery and vehicle design model

## 1.1 BatPaC V5 linkage

The most recent version of the BatPaC battery design model (version 5), developed by the Argonne National Laboratory (Nelson *et al.*, 2019), is used as the underlying product model in this case study. BatPaC is a bottom-up comprehensive battery design and cost model that is widely used in the research community to model battery costs (Duffner *et al.*, 2020*b*), and as input to LCA[1] (Peters *et al.*, 2017). Based on one energy demand parameter (pack energy (kWh) or pack capacity (Ah)), and several user-defined design battery parameters, the model is solved iteratively by varying the cell capacity and electrode thickness to match the desired battery energy. Based on the battery system solution, the bill of materials (BOM) and battery performance can be extracted. Due to its modular set-up, users are able to change specific design features at the electrode, cell, module and pack level. As such, the model has been used to calculate the cost and emissions of novel chemistries such sodium-ion (Vaalma *et al.*, 2018) and lithium oxygen batteries (Wang *et al.*, 2020). The model is peer-reviewed, well documented, and its open-access nature allows users to access all underlying calculations.

One drawback of BatPaC is that it is an Excel-based model, and the modelling of many battery designs to obtain the BOM and performance data is time-consuming. To automate this process, a Python script was developed to extract the BOM based on specific battery design parameters, allowing for the fast calculation of multiple battery designs. As illustrated in Figure 1.1, user-defined parameters are sent to the BatPaC model in Excel, which iteratively solves the model, and the bill of materials and battery pack performance parameters are returned. A wide range of parameters on the cell, module, pack and vehicle level can be adjusted. An example notebook to use the Python script can be found in the Github repository.

[1] The Argonne LCA GREET model, for instance, uses BatPaC as input to calculate the inventories of battery systems (Dai *et al.*, 2018*a*; Winjobi *et al.*, 2020).

Figures/4_Results/batpac_python.pdf

Figure 1.1: Workflow of the battery and vehicle design model.

Due to the iterative calculation of BatPaC (up to 100 iterations to solve one battery system) and the need to overwrite design parameters in Excel for each model run, the developed script takes up to 2 to 3 seconds to solve one battery system. Therefore, to reduce the total model running time, parameter steps were introduced for cathode foil (10, 14 and 18 µm), anode foil (6, 10 and 14 µm) and silicon % (0, 5 and 10 wt%). As a result, a total of 10,368 potential pack designs were solved.[2] Two output files were obtained, 1) the BOM file including the material content of all battery designs ("3_MC_materials_pack_design") and 2) the parameter file containing additional solved parameters of the battery system such as pack energy, cell size and cell capacity ("3_PAR_battery_parameters").

[2] 10,368 designs are based on 4 vehicle segments × 2 cell thicknesses × 3 cathode foil thickness × 3 anode foil thickness × 6 separator types × 8 cathode active materials (CAMs) × 3 different amounts of silicon %. Graphite type choice (synthetic or natural) does not change the product characteristics and is therefore not included in the BatPaC model run.

For all design options, several key parameters were kept the same based on default settings in BatPaC (see Table 1.1). As illustrated in the table, fast charge is included and a charging time of 9.65 min (15-75% state of charge (SOC)) is assumed based on the default values in BatPaC. The maximum positive electrode thickness was constrained to 74 µm based on Ahmed *et al.* (2021). In most cases, however, the electrode thickness is constrained in the model by the maximum current density during charging to avoid Li deposition.[3] The exception is the LMO cathode, which has a higher maximum charging current density (15 mA $cm^2$) compared to $NMC_{xyz}$, NCA and LFP materials (9 mA $cm^2$) (Nelson *et al.*, 2019), and therefore allows for thicker electrodes.

Table 1.1: Default BatPaC parameters left unchanged in each model run.

| **Parameter** | **Value** | **Unit** |
|---|---:|---|
| Vehicle type | EV | - |
| Coolant type | Liquid cooling | - |
| Calculate fast charge | Yes | - |
| Recharge time (15-75% SOC) | 9.65 | minutes |
| Negative/positive ratio after formation | 1.15 | - |
| Max positive electrode thickness | 74 | µm |
| Available battery energy | 85 | % |
| Pack housing thickness | 10 | mm |
| Module container thickness | 0.5 | mm |
| Cell container thickness | 150 | µm |
| Lenght-to-width positive electrode | 3 | - |
| Cathode ratio - active material:carbon:binder | 96:2:2 | - |
| Anode ratio - active material:carbon:binder | 95:0:5 | - |
| Anode binder | CMC-SBR | - |
| Cathode binder | PVDF | - |

Additional default parameters for all pack designs include the thickness of the polyethylene terephthalate (PET) and polypropylene (PP) in the cell, which are based on BatPaC and fixed on 30 and 20 µm respectively. The Al middle layer can be changed in the model using parameter *cell_container_al_th*. For the case study, however, this value is fixed to 100 µm based on the default values in BatPaC.

Five changes to the BatPaC model were required to include several design parameters as defined in the technology map, but not present in BatPaC. these changes refer to: 1) higher silicon percentage in the anode (10%); 2) change of default anode binder material; 3) inclusion of coated separators 4) inclusion of a vehicle model to accommodate different vehicle segments and 5) change in pack and module form factors. Following is a discussion of each of these.

[3]Incorrect battery charging rates can result in the deposition of metallic lithium on the surface of graphite particles (referred to as lithium plating), resulting in an irreversible loss of capacity (Sieg *et al.*, 2019).

| Group | Component | Direct parameter dependency |
|---|---|---|
| **Anode** | anode active material (SiO) | silicon_anode |
| | anode active material (graphite) | graphite_type |
| | anode binder (CMC) | perc_cmc_anode_binder & negative_pct_binder |
| | anode binder additive (SBR) | perc_cmc_anode_binder & negative_pct_binder |
| | anode carbon black | negative_pct_carbon_black |
| | anode current collector Cu | negative_foil_thickness |
| **Cathode** | cathode active material | electrode_pair |
| | cathode binder (PVDF) | positive_pct_binder |
| | cathode carbon black | positive_pct_carbon_black |
| | cathode current collector Al | positive_foil_thickness |
| **Cell** | cell container | |
| | cell container Al layer | cell_container_al_th |
| | cell container PET layer | cell_container_pet_th |
| | cell container PP layer | cell_container_pp_th |
| | cell group interconnect | |
| | cell terminal anode | |
| | cell terminal cathode | |
| | electrolyte | |
| | separator | |
| **Module** | gas release | |
| | module container | |
| | module electronics | |
| | module tabs | |
| | module terminal | |
| | module thermal conductor | |
| **Pack** | battery jacket | |
| | battery jacket Al | |
| | battery jacket Fe | |
| | battery jacket insulation | |
| | battery management system | |
| | busbar | |
| | coolant | |
| | cooling connectors | |
| | cooling mains Fe | |
| | cooling panels | |
| | module interconnects | |
| | module polymer panels | |
| | module row rack | |
| | pack heater | |
| | pack terminals | |

## 1.2 Overview of calculations

### *1.2.1 Active materials*

The following default BatPaC cathode active materials can be selected (either power or energy optimised), including NMC333, NMC532, NMC622, NMC811, NCA, LFP, LMO and NMC532-LMO (50:50). Anode active material choices includes natural and synthetic graphite and Si. The graphite type has no impact on the performance of the battery, but is used for comparison in the impact assessment.

In the most recent BatPaC version (Version 5), a 5 wt% Si content can be added to the anode active material, changing the anode active material capacity (mAh g$^{-1}$) accordingly. To allow for a larger amount of Si (up to 10 wt% as highlighted in the technology map), the practical anode active material capacity ($cap_{neg\_am}$) and material density, g cm$^3$ ($\rho_{neg\_am}$) parameters in BatPaC are adjusted based on Equation 1.1:

$$i_{neg\_am} = i_{gr} \times (1 - wt\_pct_{Si}) + i_{Si} \times wt\_pct_{Si} \tag{1.1}$$

where $i$ refers to the material capacity, ($cap$) and density, ($\rho$) of the graphite ($gr$) and silicon ($Si$). The default BatPaC values of 360 and 2000 mAh g$^{-1}$ were used for graphite and silicon capacity respectively and 2.24 g cm$^3$ for graphite density.[4] The density of Si, not included in the default calculation of BatPac, is 2.13 g cm$^3$ based on Greenwood *et al.* (2021). The $wt\_pct_{Si}$ in Equation 1.1 refers to the weight percentage of Si and is constrained to a value ranging between 0 and 10 wt%.

### *1.2.2 Current collector foils*

The weight of the current collector foil is based on the foil area ($A_{foil}$), the density ($\rho_{foil}$) of Cu for the anode (8.96 g cm$^3$) and Al for the cathode (2.7 g cm$^3$) and the thickness of the foil $th_{foil}$. The foil area is based on the required width and length of the positive electrode and therefore dependent on different geometric design parameters such as cell width/length ratio. The foil thickness (µm) is an adjustable parameter that can be changed in the model with the parameter `positive_foil_thickness` and `negative_foil_thickness`.

$$wt_{current\_collector\_foil} = A_{foil} \times \rho_{foil} \times th_{foil} \tag{1.2}$$

### *1.2.3 Coated and non-coated separator*

The weight of the separator ($wt_{sep}$) is calculated as the sum of the required separator area ($A_{sep}$), the density ($\rho_{sep}$) and the thickness ($th_{sep}$).

$$wt_{sep} = A_{sep} \times \rho_{sep} \times th_{sep} \tag{1.3}$$

The separator area is calculated in BatPaC based on the length ($L$) and width ($W$) of the cathode, the separator overhang ($OH$) and the bicell layers. The length and width and amount

[4] For NMC811, the default values of 345 mAh g$^{-1}$ and 2.2 g cm$^3$ for graphite were used.

of bicell layers of the cathode are based on BatPaC values. The separator overhang are changeable parameters (`sep_overhang_width` and `sep_overhang_length`), whereby the default BatPaC values of 2mm for the width and 4mm for length of the cathode are used if left unchanged.

$$A_{sep} = (L_{cath} + OH_{l,sep}) \times (W_{cath} + OH_{w,sep}) \times bicell\_layers \tag{1.4}$$

To account for the possibility of a coated separator, the default value for $\rho_{sep}$ in BatPaC was updated based on Equation 1.5.

$$\rho_{sep} = \frac{th_{sep\_film} \times \rho_{sep\_film} + th_{sep\_coating} \times \rho_{sep\_coating}}{th_{sep\_film}} \times V_{sep} \tag{1.5}$$

Thereby $V_{sep}$ is the void fraction of porosity of the separator. The value for $V_{sep}$ is based on the standard BatPaC chemistries, which is 50%. For the $\rho_{sep\_film}$, the BatPaC default value (0.9 g $cm^3$) is used, representing the $\rho$ of PP. The density of the silica-based coating layer is 1.996 g $cm^3$, assuming the coating consists of PVDF (26 wt.%), hexafluorpropylene (4 wt.%), dibutyl phthalate (40 wt.%) and silica (30 wt.%), as reported by Notter *et al.* (2010) and used in the ecoinvent 3.7.1 database.

### *1.2.4 Binder*

The value for the binder density in BatPaC is based on the density of polyvinylidene fluoride (PVDF). In this case study, however, a mixture of carboxymethyl cellulose (CMC) and styrene-Butadiene Rubber (SBR) is used for the anode binder as commonly found in current EVs (for an overview of current binder types in EVs see **??** in the appendix). To include the density of the CMC-SBR anode, the BatPaC default value is updated accordingly. A default mixture of CMC-SBR is assumed to be 60:40 and has a final density of 1.336 g/$cm^3$ (Crenna *et al.*, 2021).[5] The ratio of CMC-SBR, however, can be changed within the model with parameter `perc_cmc_anode_binder`.

### *1.2.5 Cell container*

The weight of the cell container depends on the cell format (i.e. cylindrical, prismatic or pouch). The default prismatic cell container of BatPaC is used, consisting of three different layers. The outer layer is made of polyethylene terephthalate (PET) providing strength to the container, an aluminium middle layer is used for stiffness and closure for moisture and electrolyte solvent vapors and polypropylene (PP) inner layer is used for sealing (Gallagher & Nelson, 2014). The weight of the container is based on the volume of the cell container ($V_{cell\_container}$), the thickness of each material layer ($th_{material}$) and the respective material density ($\rho_{material}$).

$$wt_{cell\_cont} = th_{material} \times \rho_{material} \times V_{cell\_container} \tag{1.6}$$

The thickness of the PET, Al and PP layer can be changed with parameters `cell_container_pet_th`, `cell_container_al_th` `cell_container_pp_th`, respectively.

[5]Based on a density of 1.59 g/$cm^3$ and 0.94 (g/$cm^3$) for CMC and SBR, respectively.

## 1.3 Vehicle model

Vehicle characteristics such as size and energy consumption influence the battery energy requirement and the corresponding battery design. To account for these aspects, a vehicle model sheet was added to BatPaC to calculate the energy storage requirement based on specific vehicle design parameters. The calculation is based on the model developed by Deng *et al.* (2017) and the underlying physics based model to estimate the energy-vehicle mass relation by Kim & Wallington (2016). As the total vehicle mass is dependent on the battery mass, Deng *et al.* (2017) established a linkage between the vehicle model with BatPaC. As illustrated in Figure 1.2, the vehicle and battery model interact by iteratively calculating the battery capacity and corresponding energy requirement for the vehicle. The model by Deng *et al.* (2017) is adapted and calibrated based on the four vehicle segments (mini, small, medium and large) as identified in the material-technology system map (see Section **??**). The following section is a description of the model and the parameters used.

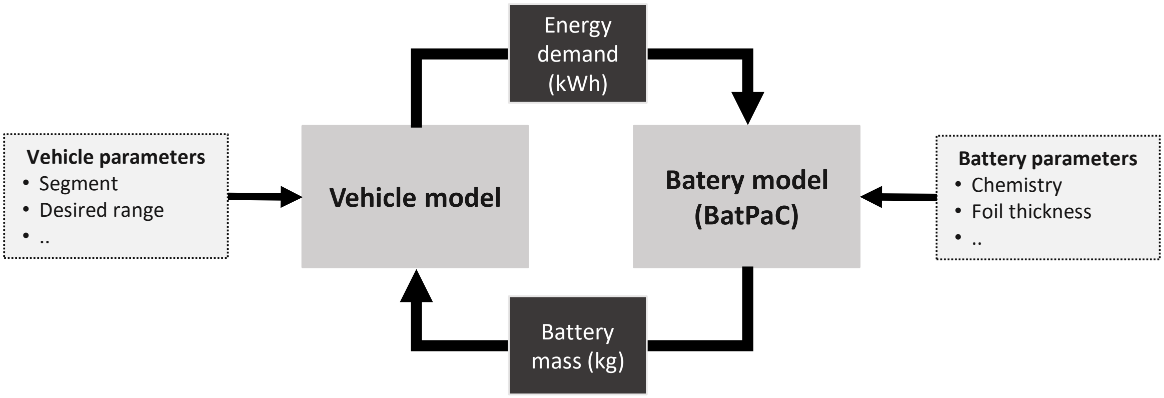


Figure 1.2: Vehicle model and BatPaC interaction. This interaction is based on the developed model by Deng *et al.* (2017).

The first step is to calculate the initial battery mass ($wt^0_{batt}$) of a pre-determined nominal battery capacity ($E^0_{nominal}$):

$$wt^0_{batt} = \frac{E^0_{nominal}}{\rho_{batt}} \tag{1.7}$$

where $\rho_{batt}$ is the gravimetric density (Wh kg$^{-1}$) of the specific battery design, calculated with BatPaC. Based on the initial battery mass, the total vehicle mass ($wt_{veh}$) can be calculated with Equation 1.8

$$wt_{veh} = wt_{batt} + wt_{glider} + wt_{motor} + wt_{transmission} \tag{1.8}$$

where the glider weight ($wt_{glider}$) is based on the mass compounding coefficient of 0.57 kg/$wt_{veh}$ and the weight of the transmission ($wt_{transmission}$) and motor ($wt_{motor}$) are calculated by multiplying the mass-power coefficients of 0.585 kg kW$^{-1}$ for the transmission and 0.9 kg kW$^{-1}$ for the motor with the power of the battery ($P_{battery}$) (Deng *et al.*, 2017). The $P_{battery}$ was calculated from the motor power ($P_{motor}$) similar to Safoutin *et al.* (2018), accounting for a motor power loss, $\eta_{motor}$, of 8% (Deng *et al.*, 2017) and an EOL power fade, $EOL_{power}$, of 20%

(Safoutin *et al.*, 2018):

$$P_{battery} = P_{motor} \times \eta_{motor} \times EOL_{power} \tag{1.9}$$

Due to the lack of available data on $P_{motor}$, data from four representative vehicle models for each segment were used which where obtained from vehicle-specific EPA testing reports (EPA, 2021*b*). These include: Smart Fortwo Electric Drive 2019 model (micro segment); Hyundai Kona Electric 2019 model (small segment); Volkswagen ID. 4 82 kWh (medium segment); Ford Mustang Mach-e (large segment). An overview of the $P_{motor}$ for each segment is presented in Table 1.3.

Table 1.3: Segment specific parameters for the vehicle model.

| **Parameter** | **Notation** | **Unit** | **Segment**[a] Micro | Small | Medium | Large |
|---|---|---|---|---|---|---|
| Rolling resistance | $A$ | $N$ | 101.86 | 110.59 | 136 | 209.4 |
| Rotation resistance | $B$ | $N/(m/s)$ | 3.42 | -1.99 | 3.73 | 2.59 |
| Aerodynamic resistance | $C$ | $N/(m/s)^2$ | 0.37 | 0.46 | 0.41 | 0.47 |
| Distance[b] | D | km | 200 | 322 | 411 | 460 |
| Auxiliary power[c] | $P_{aux}$ | W | 475 | 575 | 715 | 775 |
| Motor power[d] | $P_{motor}$ | kW | 55 | 150 | 150 | 209 |

[a] The $A$, $B$ and $C$ coefficients are based on the following vehicle models: Smart Fortwo Electric Drive 2019 model (micro); Hyundai Kona Electric 2019 model (small); Volkswagen ID. 4 82 kWh (medium); Ford Mustang Mach-e (large).
[b] Based on the average WLTP range for all vehicles of each segment as stated on EV-Database.org.
[c] Values are based on the base case of Cox *et al.* (2020).
[d] Values are based on vehicle model specific testing reports from the EPA obtained through EPA (2021*b*).

Following the mass of the vehicle, the desired mass-induced fuel consumption, here referred to as traction energy ($E_{traction}$), can be calculated with the physics-based model by Kim & Wallington (2016). Equation 1.10 calculates the $E_{traction}$ (kWh) needed for a specific driving cycle ($i$), where $i$ includes the US Environmental Protection Agency's (EPA) Urban Dynamometer Driving Schedule (UDDS) and the Highway Fuel Economy Test (HWFET):

$$E_{traction,i} = \int (Av_i + Bv_i^2 + Cv_i^3 + a_i \times v_i \times (1 - \theta \times \mu \times \eta_{charging}) \times wt_{veh})dt \tag{1.10}$$

$v_i$ and $a_i$ are the driving speed (m/s) and acceleration (m/s$^2$) respectively for each driving cycle $i$. The values for these are obtained from Kim & Wallington (2016) and Deng *et al.* (2017). $A$, $B$ and $C$ are the rolling ($N$), rotating (N/(m s)) and aerodynamic resistance (N/(m/s)$^2$) coefficient respectively. These coefficients, also referred to as the target coefficients, are used by the EPA to calibrate the resistance of the dynamometer rollers' for fuel economy testing and are publicly available for all registered vehicles in the US (EPA, 2021*a*). Target coefficients for the four representative vehicles were obtained as listed in Table 1.3. The final parameters in Equation 1.10 were used to calculate the kinetic energy captured via the regenerative braking system. This was obtained by reducing the mass of the vehicle by the sum of the braking to kinetic energy ratio ($\theta$), the regenerative braking efficiency ($\mu$) and the charging efficiency ($\eta_{charging}$). The average values for $\mu$ (5%) and $\theta$ (0.74 UDDS and 0.41 HWFET) as recommend by Kim & Wallington (2016) were used for all vehicle segments. The charger efficiency, ($\eta_{charging}$) is set to 90% for all battery designs as commonly applied in LIB LCA studies (Peters *et al.*, 2017).

Based on the required traction energy requirement, the total nominal battery energy ($E^{required}_{nominal}$) was calculated with Equation 1.11 to 1.13 based on Deng *et al.* (2017):

$$E_{discharged} = \sum_i \frac{a_i \times D}{\int v_i^{dt}} \times \frac{E_{traction,i}}{\eta_{motor} \times \eta_{transmission}} + D \times P_{aux} \times (a\frac{\int dt_i}{\int v_i}) \tag{1.11}$$

$$E_{stored} = \frac{E_{discharged}}{\eta_{discharging}} \tag{1.12}$$

$$E^{required}_{nominal} = \frac{E_{stored}}{UR} \tag{1.13}$$

Equation 1.11, calculates the total discharged energy for a required range ($D$) as the sum of the energy demand from auxiliary devices (heating, cooling, etc.), $P_{aux}$, and the traction energy demand ($E_{traction}$) for both the urban and highway driving cycle ($i$) as calculated in Equation 1.10. The required distance for each vehicle segment is based on the average range of all currently available BEV models for each segment, as reported on the EV-Database (2021). The Worldwide harmonized Light vehicles Test Procedure (WLTP) values for each available BEV model for all segments were used. As highlighted in Table 1.3, this resulted in a desired range of 200, 322, 411 and 460 km for micro, small, medium and large vehicles respectively.

To include the differences in $P_{aux}$ for different vehicle sizes (e.g. heating demand is higher for larger vehicles), the base case power demand for mini, small, medium and large vehicles as reported by Cox *et al.* (2020) were used. This includes a power demand for base electrical equipment (75W) and a segment-specific heat and cooling demand (see Table 1.3). Furthermore, the traction energy demand ($E_{traction}$) in Equation 1.11, is adjusted to account for the efficiency of the motor ($\eta_{motor}$, 0.89) and transmission ($\eta_{transmission}$, 0.93) (Deng *et al.*, 2017). $a$ in Equation 1.11 refers to the share of city or highway driving for distance $D$. The standard EPA fuel economy testing ratio of 55% city and 45% highway driving were used. A discharge efficiency ($\eta_{discharging}$) is 90% based on the charging efficiency. A complete list of all parameters used in the vehicle model can be found from Table **??** in Appendix B.

## 1.4 Form factors

To make sure the designed pack in BatPaC fits the vehicle size, pack size parameters were defined for all vehicle types. In BatPaC, the battery length, width and height cannot be directly changed, but instead are determined by four main parameters on the cell, module and pack level, see Figure 1.3. These include the total modules per row, the rows of modules, total cells per module, and the thickness of the cell.

Figures/4_Results/format_design_parameters.pdf

Figure 1.3: BatPaC pack, module and cell format parameters.

The pack width constraint was determined by the width of the vehicle and additional safety space of 305 mm per side, as used by Sankaran & Venkatesan (2021). For height, a standard value of 160 mm was used based on the reviewed vehicle models by Sankaran & Venkatesan (2021). Based on the pack size constraints, the corresponding BatPaC parameters were adjusted manually to find the best fit (see Figure **??** in the Appendix for an overview). For the pack length this included changing the modules per row, cells per row and cell thickness and the rows of modules to change the width. The parameters resulting in the best fit for each segment are listed in Table 1.4.

Table 1.4: Width and wheelbase of representation vehicles. Data obtained from EV-Database (2021)

| | **Micro** | **Small** | **Medium** | **Large** |
|---|---|---|---|---|
| Max pack length (mm) | 1,217 | 1,690 | 1,801 | 1,940 |
| Max pack width (mm) | 1,053 | 1,190 | 1,240 | 1,271 |
| Max pack height (mm) | 160 | 160 | 160 | 160 |
| Cells per module (20 mm cell) | 12 | 12 | 16 | 14 |
| Cells per module (40 mm cell) | 6 | 6 | 8 | 7 |
| Modules per row | 4 | 6 | 5 | 6 |
| Rows of modules | 2 | 4 | 4 | 3 |
| Total cells (20 mm cell) | 96 | 192 | 320 | 252 |
| Total cells (40 mm cell) | 48 | 96 | 160 | 126 |

# 2. Supplementary information material and energy flow layer

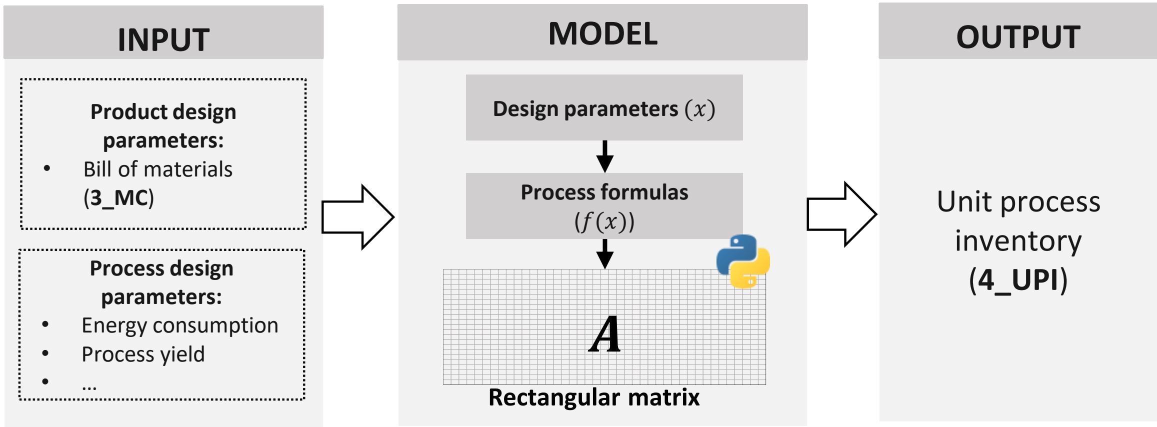


Figure 2.1: Workflow of the foreground material and energy flow model.

## 2.1 Energy consumption battery production

Early LCA studies of battery production such as Ellingsen *et al.* (2014), Notter *et al.* (2010) or Dunn *et al.* (2015) were based on pilot-scale facilities or modelled estimates. More recently, several studies published data on energy consumption based on industry sources, see Table 2.1. However, large discrepancies in energy consumption can be observed between studies. Production capacity in general has a large impact on the energy consumption (Davidsson Kurland, 2019; Jinasena *et al.*, 2021; Dai *et al.*, 2019*a*), as can also be observed in Table 2.1.

The giga-scale facilities energy consumption are all in a similar range, whereby Sun *et al.* (2020) reports the lowest energy consumption levels (28 $Wh^{-1}$ per $Wh^{-1}$ of cell energy) for a 30 GWh operating plant in China. A relatively high-energy consumption, 92 $Wh^{-1}$ per $Wh^{-1}$ of cell energy, can be observed from the study by Chordia *et al.* (2021). The underlying data, obtained from the technical reports from a facility to be build in Sweden, is based on a simulation model. Further process optimisation of an actual operating plant is expected to improve energy efficiency (e.g. the authors cite the example of cell formation, which could be improved by up to 40%). Furthermore, the authors include several additional processes such as "cell container manufacturing" (2.76 Wh $Wh^{-1}$), "waste water treatment" (6.99 Wh $Wh^{-1}$) and facility operations and utilities (27.15 Wh $Wh^{-1}$) that none of the other studies report.

Due to the detail of the process steps, calculation and availability of the data, here the energy consumption by Degen & Schütte (2022) is adopted. The authors base their data on the factory plans of a 7 GWh cylindrical manufacturing plant in German and calculate the energy consumption from machine specifications of different manufacturers, which include reliable statements about energy consumption.[1]

The process energy consumption calculation is adopted from Degen & Schütte (2022). The energy input ($E$), for both electricity and gas ($n$) for each battery production process ($bp$) is

[1]The cell form format in the study by Degen & Schütte (2022) is cylindrical while the cell used in the product model and BatPaC is prismatic. However, as pointed out by the authors, the cell form factor has little influence on the energy consumption as the resulting changes occur during cell assembly, which has only a small impact on the overall energy consumption.

Table 2.1: Industry based reported energy consumption data, including heating, electricity and cooling for battery cell production steps. Unit is Wh per 1 Wh of cell energy. Data updated from Jinasena *et al.* (2021).

| | **Yuan *et al.* (2017)** | **Kim *et al.* (2016)** | **Pettinger & Dong (2016)** | **Dai *et al.* (2017)** | **Degen & Schütte (2022)** | **Chordia *et al.* (2021)** | **Sun *et al.* (2020)** |
|---|---|---|---|---|---|---|---|
| **Mixing** | 0.88 | - | 2.64 | - | 0.13 | - | 1 |
| **Coating** | 51.2 | - | 15.42 | 15.6-19.7 | 11.02 | - | - |
| **Calendering** | 3.04 | - | 5.97 | - | 0.53 | - | - |
| **Stacking** | 6.16 | - | 5.97 | - | 0.41 | - | - |
| **Final drying** | - | - | 5.97 | - | 1.61 | 39.42[a] | 12.7 |
| **Filling** | 4.72 | - | 1.53 | - | 1.59 | 2.76[b] | - |
| **Formation** | 0.56 | - | 2.92 | 1.11 | 13.54 | 14.77 | 3 |
| **Dry room** | 31.2 | - | - | 17.5-26.9 | 10.68 | - | 11.7 |
| **Pack assembly** | - | - | - | - | - | - | 1 |
| **Other** | 8.48 | - | 5.56 | - | 1.98 | 34.81 | - |
| **Total** | 106 | 147[c] | 46 | 34-47 | 41.49 | 92[c] | 28 |
| **Annual capacity** (GWh | 0.02 | 0.06[b] | 0.08 | 2 | 8 | 16 | 30 |

[a] Quantity refers to total cathode and anode production energy.
[b] Includes electrolyte mixing, feeding and cell assembly
[b] Calculated based on capacity of 1 million cells per year. Pack is 23 kWh and includes 430 cells.
[c] Excluded energy consumption from cathode active material production.
[d] Includes module and battery assembly which only represent a small proportion of energy consumption (Sun *et al.*, 2020). Calculated based on the reported primary energy of 120 MJ kg−1 battery, battery weight and capacity of 303 kg and 24 kWh and a primary to electric energy conversion factor of 0.35 as used by the authors.

calculated with:

$$\mathbf{E}_{n,bp} = -\frac{P_{bp,e} \times prod\_time_{yr}}{prod\_volume_{yr}} \tag{2.1}$$

$P_{bp}$ is the machine power for each production step and $prod\_time$ the total hours machines need to run to produce the annual cell capacity ($prod\_volume_{yr}$). The $product\_time$ and $prod\_volume_{yr}$ are 8,760 h yr$^{-1}$ and 883.01 MWh yr$^{-1}$ respectively.

The hourly machine power ($P_{bp,n}$), including electricity and heat, for each production step is based on the nominal machine power ($P_{nom,bp}$), the total machines required ($M_{bp}$ for each process, the hourly producible cell capacity of each process at nominal power ($prod\_volume_{hr,bp}$)) and total cell output per hour ($prod\_volume_{hr}$)):

$$P_{bp,n} = \frac{P_{nom,bp} \times M_{bp}}{prod\_volume_{hr,bp} \times prod\_volume_{hr}} \tag{2.2}$$

Degen & Schütte (2022) obtained the nominal machine power for each process steps from three different machine manufacturers with slightly different reported power requirements. The authors use the average of this to calculate the total energy requirements. Here a low, average and high scenario is established based on these values. Table 2.3 presents the used nominal machine power ($P_{nom,bp}$) for a low, average and high scenario.

Following this, the electricity and gas consumption for each production process can be calculated. The final result, however, presents the process energy consumption per kWh of cell. A multiplication of this by the capacity of cells with different characteristics (i.e. higher capacity) would overestimate the energy consumption. Instead, cell weight is used here to calculate the energy consumption per process. Degen & Schütte (2022) do not disclose cell weight but state that a cell (standard cylindrical 21700 format) throughput of 12,000 cells hr$^{-1}$ is equal to 100.8 kWh. Assuming an average weight for a 21700 cell of 67 gr (reported weight ranges from 63 to 70 gr (Quinn *et al.*, 2018; Lain *et al.*, 2019)), the energy consumption per kg cell can be estimated accordingly.

Table 2.3: The nominal machine power (kW) requirement for each battery production step in a low, medium and high scenario. Data obtained from Degen & Schütte (2022) and based on three manufacturers. The scenarios highlight the minimum, average or maximum value for each production process across the three manufacturers.

| **Process** | **Nominal machine power (kW)** | | | | | |
|---|---|---|---|---|---|---|
| | ***Electricity*** | | | ***gas*** | | |
| | *Low* | *Medium* | *High* | *Low* | *Medium* | *High* |
| Mixing | 15 | 19 | 30 | 0 | 0 | 0 |
| Coating and drying | 60 | 74 | 95 | 750 | 823 | 875 |
| Calendaring | 55 | 60 | 70 | 0 | 0 | 0 |
| Slitting | 40 | 45 | 50 | 0 | 0 | 0 |
| Vacuum drying | 5 | 7 | 10 | 200 | 210 | 230 |
| Winding | 15 | 24 | 30 | 0 | 0 | 0 |
| Assembly | 150 | 160 | 175 | 0 | 0 | 0 |
| Washing | 160 | 198 | 225 | 0 | 0 | 0 |
| Formation | 850 | 994 | 1100 | 20 | 25 | 30 |
| Ageing | 0 | 0 | 0 | 30 | 39 | 55 |
| Testing | 100 | 100 | 100 | 0 | 0 | 0 |
| Material handling | 180 | 170 | 250 | 0 | 0 | 0 |
| Drying rooms | 175 | 150 | 164 | 872 | 912 | 950 |

The used energy consumption in this study are provided in Table 2.4. As illustrated in the table, all energy consumption units are based on cell mass, except for the formation step and the module and pack assembly. During the formation step, the cell is charged and discharged (see also Section 2.10), and the cell capacity a better estimate to calculate the energy consumption. The module and pack assembly consumption are not included in the data by Degen & Schütte (2022) but instead taken from Sun *et al.* (2020). This data is converted from kWh/kWh to Wh/kg of battery pack based on the reported pack density of 0.115 kWh kg$^{-1}$ in the study of Degen & Schütte (2022). Furthermore, although scrap rates are not disclosed by Degen & Schütte (2022), it is assumed that this data includes a 5% cell scrap rate during cell testing (Duffner *et al.*, 2021; Nelson *et al.*, 2019). The total energy consumption is adjusted accordingly.

Table 2.4: Electricity and gas consumption for each cell production process based on Degen & Schütte (2022) and module and pack assembly based on Sun *et al.* (2020). Original data units converted from kWh to kg based on a cell specific energy of 0.124 kWh $kg^{-1}$ and 0.115 kWh $kg^{-1}$ for module and pack assembly. It is assumed that the data by Degen & Schütte (2022) includes a 5% cell scrap rate after the testing stage. The presented data excludes this scrap rate from the mixing to testing phase.

| **Process** | **Unit** | **Electricity** | | | **Natural gas** | | |
|---|---|---|---|---|---|---|---|
| | | *Low* | *Med.* | *High* | *Low* | *Med.* | *High* |
| Mixing | kWh $kg^{-1}$ cell | 0.012 | 0.015 | 0.024 | 0.000 | 0.000 | 0.000 |
| Coat & dry | kWh $kg^{-1}$ cell | 0.086 | 0.106 | 0.137 | 1.079 | 1.184 | 1.259 |
| Calendaring | kWh $kg^{-1}$ cell | 0.062 | 0.068 | 0.079 | 0.000 | 0.000 | 0.000 |
| Slitting | kWh $kg^{-1}$ cell | 0.018 | 0.020 | 0.023 | 0.000 | 0.000 | 0.000 |
| Vacuum drying | kWh $kg^{-1}$ cell | 0.005 | 0.007 | 0.010 | 0.193 | 0.202 | 0.222 |
| Winding | kWh $kg^{-1}$ cell | 0.017 | 0.028 | 0.035 | 0.000 | 0.000 | 0.000 |
| Cell assembly | kWh $kg^{-1}$ cell | 0.175 | 0.186 | 0.204 | 0.000 | 0.000 | 0.000 |
| Washing | kWh $kg^{-1}$ cell | 0.186 | 0.230 | 0.262 | 0.000 | 0.000 | 0.000 |
| Formation | kWh $kWh^{-1}$ cell | 8.011 | 9.425 | 10.367 | 0.188 | 0.236 | 0.283 |
| Ageing | kWh $kg^{-1}$ cell | 0.000 | 0.000 | 0.000 | 0.035 | 0.045 | 0.064 |
| Testing | kWh $kg^{-1}$ cell | 0.117 | 0.117 | 0.117 | 0.000 | 0.000 | 0.000 |
| Material handling | kWh $kg^{-1}$ cell | 0.221 | 0.209 | 0.307 | 0.000 | 0.000 | 0.000 |
| Drying rooms | kWh $kg^{-1}$ cell | 0.215 | 0.184 | 0.201 | 1.070 | 1.119 | 1.165 |
| Pack assembly | kWh kWh $^{-1}$ pack | 0.115 | 0.115 | 0.115 | - | - | - |

## 2.2 Inventory active material mixing

In the first production step, the anode and cathode active materials are mixed with the binder, a conductive agent (carbon black) and binder solvent to obtain a wet slurry. The mixture ratio are based on Nelson *et al.* (2019) and include active material, binder and carbon black ratios of 96:2:2 and 95:0:5 for the cathode and anode respectively. The inventory for the active material mixing process is highlighted in table 2.10.

For the CMC-SBR anode binders, water is used as a solvent, while for the cathode slurry and PVDF binder, N-methyl-2-pyrrolidone (NMP) is used (Kwade *et al.*, 2018; Peters & Weil, 2018; Dai *et al.*, 2019*a*). The total binder solvent requirement is based on the binder:solvent ratio of 1:24 as used by Nelson *et al.* (2019). The solvents are evaporated during the coating and drying process, where water is lossed to the environment and most NMP is recovered and recycled (Nelson *et al.*, 2019; Bryntesen *et al.*, 2021). Only the evaporated NMP that needs to be replaced is accounted for, similar to Notter *et al.* (2010), Crenna *et al.* (2021) and the BatPaC cost model. The BatPaC NMP recovery rate of 99.5% is used, the same quantity used by Crenna *et al.* (2021).

All quantities are based on the material content of the specific battery design determined in the battery design module and the process yield parameters. The process yield parameters for materials $m$ in the anode and cathode mixing process is based on the product of the electrode yield parameters ($py_{i,electrode}$) across all relevant processes ($i$) including: material mixing ($py_{mix}$), slurry coating ($py_{coat}$), electrode slitting ($py_{slit}$), cell stacking ($py_{stack}$) and cell formation and ageing ($py_{age}$).

Energy consumption for the mixing step ($electricity_{mixing}$) only consist of electricity required for the mixer. In the energy consumption data obtained from Degen & Schütte (2022), the authors do not differentiate between cathode and anode mixing. However, different electricity consumption rate can be expected due to the material properties and mixing requirements. Here a 65:35 ratio of electricity consumption for the anode and cathode material mixing based on a model of the mixing time and material properties of anode and cathode powders (NMC333 and graphite) by Jinasena *et al.* (2021). The electricity consumption is only adjusted for the cell yield rate.

Table 2.5: Process inventory for anode active material mixing for 1 battery pack

| Description | Quantity/function | Unit | Inventory |
|---|---|---|---|
| **Input: materials** | | | |
| Active material | $anode\_am_m / \prod_i py_{i,electrode}$ | kg | Section 3.1 |
| Binder (CMC) | $anode\_binder_{cmc} / \prod_i py_{i,electrode}$ | kg | Section 3.6 |
| Binder (SBR) | $anode\_binder_{sbr} / \prod_i py_{i,electrode}$ | kg | Section 3.6 |
| Binder solvent | $24^{a} * \sum_{sbr,cmc} anode\_binder / \prod_i py_{i,electrode}$ | $m^3$ | Section 3.6 |
| Carbon black | $anode\_cb / \prod_i py_{i,electrode}$ | kg | Section 3.6 |
| **Input: process** | | | |
| Electricity | $0.35 * wt\_cell * electricity_{mixing} / py_{cell}$ | kWh | Market for electricity, medium voltage |
| **Output: reference product** | | | |
| Anode slurry | $\sum anode_{am,binder,cb,solvent} \prod_i py_{i,electrode}$ | kg | |
| **Output: waste** | | | |
| Waste active material | $anode\_am_m * py_{mix}$ | kg | |
| Waste binder (CMC) | $anode\_binder_c mc * py_{mix}$ | kg | |
| Waste binder (SBR) | $anode\_binder_s br * py_{mix}$ | kg | |
| waste carbon black | $anode\_cb * py_{mix}$ | kg | |

[a] 1:24 binder-solvent ratio based on Nelson *et al.* (2019).

Table 2.6: Process inventory for cathode active material mixing for 1 battery pack

| Description | Quantity/function | Unit | Inventory |
|---|---|---|---|
| **Input: materials** | | | |
| Active material | $cathode\_am_m/\prod_i py_{i,electrode}$ | kg | Section 3 |
| Binder (PVDF) | $cathode\_binder/\prod_i py_{i,electrode}$ | kg | Section 3.6 |
| Binder solvent (NMP) | $24^a * cathode\_binder/\prod_i py_{i,electrode} * (1 - py_{nmp})^b$ | kg | Section 3.6 |
| Binder solvent (NMP) recycled | $24^a * cathode\_binder/\prod_i py_{i,electrode} * py_{nmp}{}^b$ | kg | Section 3.6 |
| Carbon black | $cathode\_cb/\prod_i py_{i,electrode}$ | kg | Section 3.6 |
| **Input: process** | | | |
| Electricity | $0.65 * wt\_cell * electricity_{mixing}/py_{cell}$ | kWh | Market for electricity, medium voltage |
| **Output: reference product** | | | |
| Cathode slurry | $\sum cathode_{am,binder,cb,solvent} \prod_i py_{i,electrode}$ | kg | |
| **Output: waste** | | | |
| Waste active material | $cathode\_am_m * py_{mix}$ | kg | |
| Waste binder (PVDF) | $cathode\_binder_c mc * py_{mix}$ | kg | |
| waste carbon black | $cathode\_cb * py_{mix}$ | kg | |

[a] 1:24 binder-solvent ratio based on Nelson *et al.* (2019).
[b] 99.5% recovery rate of NMP.

## 2.3 Inventory electrode coating and drying

After active material mixing, the electrode current collectors are coated with the slurry and dried to fix the coating to the surface of the current collector (Bryntesen *et al.*, 2021). During the drying process, the binder solvent is evaporated, whereby only the high value NMP is internally recovered and reused. As mentioned above, the assumed NMP recovery rate is 99.5%. The small fraction of non-recovered NMP is evaporated to the air and modelled as non-methane volatile organic compounds (NMVOC) (Kallitsis *et al.*, 2020; Crenna *et al.*, 2021). Evaporated water is treated as waste flow, similar to Crenna *et al.* (2021). The requirement for the electrode current collector is dependent on the foil thickness and therefore based on the $anode/cathode\_foil$ parameter obtained from the product model.

The energy consumption of cathode drying is typically higher due to the lower drying rate and higher solvent mass (NMP as compared to water) (Jinasena *et al.*, 2021). The modelled values for the coating process by Jinasena *et al.* (2021) of an NMC333 cathode with an NMP solvent and graphite anode with a water solvent are here used as proxy to determine the ratio between the anode-cathode coating and drying energy consumption. The original energy consumption (both electricity and gas) by Sun *et al.* (2020) are therefore multiplied by this ratio (24% for the anode and 76% for the cathode).

Table 2.7: Process inventory for anode coating and drying of 1 battery pack

| **Description** | **Quantity/function** | **Unit** | **Inventory** |
|---|---|---|---|
| **Input: materials** | | | |
| Anode slurry | $wt\_anode\_slurry$ | kg | Section 2.2 |
| Current collector | $wt\_anode\_foil$ | kg | Section 3.8 |
| **Input: process** | | | |
| Electricity | $0.24 * wt\_cell * electricity_{coat}/py_{cell}$ | kWh | Market for electricity, medium voltage |
| Heat | $0.24 * wt\_cell * heat_{coat}/py_{cell}$ | MJ | Market group for heat, district or industrial, natural gas[RER] |
| **Output: reference product** | | | |
| Coated anode | $anode\_slurry + anode\_foil - waste$ | kg | |
| **Output: waste** | | | |
| Waste water | $anode\_solvent * (1 - py\_am\_mixing)$[a] | $m^3$ | Wastewater, average [Europe w/o CH] |
| Waste foil | $\mathrm{py}_{foil,coat} * anode\_foil$ | kg | Waste handling |
| Waste slurry | $\mathrm{py}_{slurry,coat} * anode\_slurry$ | kg | Waste handling |

[a] Accounts for binder yield loss during mixing.

Table 2.8: Process inventory for cathode coating and drying of 1 battery pack

| Description | Quantity/function | Unit | Inventory |
|---|---|---|---|
| **Input: materials** | | | |
| Slurry | $wt\_cathode\_slurry$ | kg | Section 2.2 |
| Current collector | $wt\_cathode\_foil$ | kg | Section 3.8 |
| **Input: process** | | | |
| Electricity | $0.76 * wt\_cell * electricity_{coat}/py_{cell}$ | kWh | Market for electricity, medium voltage |
| Heat | $0.76 * wt\_cell * heat_{coat}/py_{cell}$ | MJ | Market group for heat, district or industrial, natural gas [RER] |
| **Output: reference product** | | | |
| Coated cathode | $cathode\_slury + cathode\_foil - waste$ | kg | |
| **Output: waste** | | | |
| NMP waste | $cathode\_binder * (py\_am\_mixing)^{a}$ | kg | NMP recovery |
| Waste foil | $\mathrm{py}_{foil,coat} * cathode\_foil$ | kg | Waste handling |
| Waste slurry | $\mathrm{py}_{slurry,coat} * cathode\_slurry$ | kg | Waste handling |

[a] Accounts for binder lost during mixing.

### 2.4 Inventory calendering and electrode slitting

The dried electrodes are compressed between two calender rollers and slit to the desired size. The calendering process does not require any material inputs or produce waste. In the slitting process, the coated electrodes are slit into strips and into individual electrodes. As the total foil area is larger than the coated area, foil scrap (around 8%) during the process is higher than the coating layer (around 1%) (Nelson *et al.*, 2019). The electricity consumption for the calendering and slitting process are equally divdied between the cathode and anode and only adjusted for cell process yield.

Table 2.9: Process inventory for cathode/anode electrode slitting

| Description | Quantity/function | Unit | Inventory |
|---|---|---|---|
| **Input: materials** | | | |
| Coated electrode | $coated\_anode, cathode$ | kg | Section 2.3 |
| **Input: process** | | | |
| Electricity | $0.5 * wt\_cell * electricity_{slit}/py_{cell}$ | kWh | Market for electricity, medium voltage |
| **Output: reference product** | | | |
| Slitted electrodes | $coated\_anode, cathode - waste$ | | |
| **Output: waste** | | | |
| Waste current collector | $cathode, anode\_foil * py_{foil,slitting}$ | kg | Waste handling |
| Waste coated electrode | $coated\_anode, cathode * py_{slurry,slitting}$ | kg | Waste handling |

## 2.5 Inventory final electrode drying

After slitting, the electrodes are vacuum dried to remove any moisture in the electrodes (Nelson *et al.*, 2019). Energy consumption includes electricity and gas for heating. The final drying process for both anode and cathode is modelled as a single process.

Table 2.10: Process inventory for final electrode drying

| Description | Quantity/function | Unit | Inventory |
|---|---|---|---|
| **Input: materials** | | | |
| Slitted anode | $slitted\_anode$ | kg | Section 2.4 |
| Slitted cathode | $slitted\_cathode$ | kg | Section 2.4 |
| **Input: process** | | | |
| Electricity | $wt\_cell * electricity_{drying}/py\_cell$ | kWh | Market for electricity, medium voltage |
| Heat | $wt\_cell * heat_{drying}/py\_cell$ | MJ | Market group for heat, district or industrial, natural gas |
| **Output: reference product** | | | |
| Dried electrode | $slitted\_anode + slitted\_cathode$ | kg | |

## 2.6 Inventory cell stacking

Cell stacking is the first of four steps in assembling the cell. The electrodes are wound together with the separator sheet, forming the jelly roll (Warner, 2015). The required amount of separator is based on the specific separator foil, optional coating thickness requirements, and the process yields in cell stacking and the final cell formation. Manufacturing scrap for both the electrodes and separator are included.

Table 2.11: Process inventory for cell stacking

| Description | Quantity/function | Unit | Inventory |
|---|---|---|---|
| **Input: materials** | | | |
| Electrode | $wt\_dried\_electrode$ | kg | Section 2.5 |
| Separator | $wt\_separator/\prod_i py_{i,separator}$ | kg | Section 3.9 |
| **Input: process** | | | |
| Electricity | $wt\_cell * electricity_{winding}/py\_cell$ | kWh | Market for electricity, medium voltage |
| **Output: reference product** | | | |
| Jelly roll | $wt\_separator + wt\_electrode - waste$ | kg | |
| **Output: waste** | | | |
| Separator waste | $wt\_separator * (1 - py_{separator,stack})$ | kg | Waste handling |
| Anode electrode waste | $wt\_separator * (1 - py_{separator,stack})$ | kg | Waste handling |
| Cathode electrode waste | $wt\_separator * (1 - py_{separator,stack})$ | kg | Waste handling |

## 2.7 Inventory terminal welding

After stacking, the current collector and tabs are welded together. The tab materials are the same as the current collectors. The weight of the tabs are based on the specific cell design as modelled in BatPaC and the final cell yield rate ($py_{cell}$). No scrap rates during the process are assumed. Energy requirement are also not included due to a lack of data.

Table 2.12: Process inventory for cell terminal welding

| Description | Quantity/function | Unit | Inventory |
|---|---|---|---|
| **Materials** | | | |
| Jelly roll | $jelly\_roll$ | kg | Section 2.6 |
| cell terminal anode | $cell\_terminal\_anode/py_{cell}$ | kg | Section 3.13 |
| cell terminal cathode | $cell\_terminal\_cathode/py_{cell}$ | kg | Section 3.13 |
| **Output** | | | |
| Welded jelly roll | $jelly\_roll + terminals$ | kg | |

## 2.8 Inventory enclosing jelly roll

The jelly rolls are enclosed in the cell container.The cell container is purchased as finished components (Nelson *et al.*, 2019) and the inventory is described below. Energy requirements and scrap during the enclosing process are not included.

Table 2.13: Process inventory for cell enclosing

| Description | Quantity/function | Unit | Inventory |
|---|---|---|---|
| **Materials** | | | |
| Welded jelly rol | $welded\_jelly\_roll$ | kg | Section 2.7 |
| cell container | $cell\_container/py_{cell}$ | kg | Section 3.12 |
| **Output** | | | |
| Enclosed cell | $welded\_jelly\_roll + cell\_container$ | kg | |

## 2.9 Inventory electrolyte filling and cell sealing

Electrolyte is added to the enclosed cell and sealed based on crimping, beading or welding methods (for prismatic and cylindrical cells) (Jinasena *et al.*, 2021). The quantity of electrolyte is based on the specific battery design and the process yield during filling and cell formation. Energy consumption for the electrolyte filling and cell sealing are based on the data for cell assembly and washing from Degen & Schütte (2022). In addition, as this is the final process occuring in a dry room environment (dry room processes include part of vacuum drying, cell stacking, welding, cell enclosing and washing), electricity and gas to operate the dehumication unit are allocated to this process.

Table 2.14: Process inventory for electrolyte filling and cell enclosing

| Description | Quantity/function | Unit | Inventory |
|---|---|---|---|
| **Materials** | | | |
| Enclosed cell | $enclosed\_cell$ | kg | Section 2.8 |
| Electrolyte | $electrolyte\ py_{electrolyte,filling} * py_{cell}$ | kg | Section 3.11 |
| **Input: process** | | | |
| Electricity assembly, | $wt\_cell * electricity_{assembly}/py\_cell$ | kWh | Market for electricity, medium voltage |
| Electricity dry room | $wt\_cell * electricity_{dryroom}/py\_cell$ | kWh | Market for electricity, medium voltage |
| Heat dry room | $wt\_cell * heat_{dryroom}/py\_cell$ | kWh | Market for electricity, medium voltage |
| **Output** | | | |
| Electrolyte waste | $electrolyte * py_{electrolyte,filling}$ | kg | |
| Unformatted cell | $electrolyte + enclosed\_cell - waste$ | kg | |

### 2.10 Inventory cell formation

During the formation phase, the final step in the cell assembly, the cell is charged to produce the interface layer (solid electrolyte interface (SEI)) and the functioning of the cell is tested through formation cycling and charge-retentions tests (Pettinger *et al.*, 2018; Nelson *et al.*, 2019). Around 5% of the cells typically fail the quality testing (Duffner *et al.*, 2021). Energy consumption is based on the reported values for formation, ageing and testing by Degen & Schütte (2022). Electricity consumption for cell formation and testing is based on the pack capacity rather than the cell weight, assuming all electricity is used for charge and discharge cycling of the cell.

Table 2.15: Process inventory for cell formation

| Description | Quantity/function | Unit | Inventory |
|---|---|---|---|
| **Materials** | | | |
| Enclosed cell | $enclosed\_cell$ | kg | Section 2.8 |
| **Processes** | | | |
| Electricity | $cell\_capacity * electricity_{formation}/py_{cell}$ | kWh | Market for electricity, medium voltage |
| Heat | $wt\_cell * heat_{formation}/py_{cell}$ | MJ | Market group for heat, district or industrial, natural gas |
| **Output** | | | |
| Waste cell | | kg | |
| Cell | $enclosed\_cell * py_{cell,formation}$ | kg | |

### 2.11 Inventory module and battery assembly

In the final process step, the accepted cells from the formation phase are assembled in modules and packs (modelled as a single process). An aluminium conduction channel is added to each side of the cell for heat rejection. The cells are then placed into the module packaging, consisting of an air-tight aluminium housing. The size and weight of the module housing is dependent on the specific geometric design features and the thickness of the housing. The module electronics, module terminals, conductors and spacers for gas release are added. Finally, the finished modules are placed into the battery pack jacket, including the battery management system (BMS), the coolant, busbars, module compression plates, pack heaters, interconnects and pack terminals. All these components are assumed to be manufactured outside the battery production factory, and more details for each component are discussed below.

The total electricity consumption for module and battery assembly is 1 kWh/kWh battery (0.115 kWh/kg) based on Sun *et al.* (2020). Electricity requirement for inter-process materials handling as stated by Degen & Schütte (2022) is also allocated to this process to include the overall electricity consumption for material handling. To account for all pack materials (not just the cell), the electricity consumption stated by Degen & Schütte (2022) is multiplied by the total pack weight. No further scrap is assumed to occur at this stage. To account for the construction of the battery factory, an infrastructure process is added in the module and battery assembly process similar to Crenna *et al.* (2021) and Ellingsen *et al.* (2014).

Table 2.16: Process inventory for module and battery assembly

| **Description** | **Quantity/function** | **Unit** | **Inventory** |
|---|---|---|---|
| **Materials** | | | |
| Cell | *cell* | kg | Section 2.10 |
| Cell interconnect | *cell_interconnect* | kg | Section 3.20 |
| Module terminals | *module_terminal* | kg | Section 3.15 |
| Module tabs | *module_tabs* | kg | ADD |
| Module panels | *module_panels* | kg | ADD |
| Module row rack | *module_rack* | kg | ADD |
| thermal conductor | *module_thermal_conductor* | kg | Section 3.17 |
| Gas release | *gas_release* | kg | Section 3.18 |
| Module container | *module_container* | kg | Section 3.14 |
| Module electronics | *module_electronics* | kg | Section 3.19 |
| Pack housing | *battery_jacket* | kg | Section 3.21 |
| Management system[a] | *battery_management_system* | kg | Section 3.31 |
| Busbar | *busbar* | kg | Section 3.26 |
| Coolant | *coolant* | kg | Section 3.27 |
| Cooling tubes | *cooling_mains* | kg | ADD |
| Cooling connectors | *cooling_connectors* | kg | ADD |
| Cooling panels | *cooling_panels* | kg | ADD |
| Compression plates | *module_compression_plates* | kg | Section 3.22 |
| Interconnects | *module_interconnects* | kg | Section 3.23 |
| Heater | *pack_heater* | kg | Section 3.25 |
| Terminals | *pack_terminals* | kg | Section 3.24 |
| **Processes** | | | |
| Electricity assembly | $battery\_weight * electricity_{assembly}$ | kWh | Market for electricity, medium voltage |
| Electricity material handling | $battery\_weight * electricity_{handling}$ | kWh | Market for electricity, medium voltage |
| **Infrastructure** | | | |
| Infrastructure | $1.41 \times 10^{-9}$ | unit | Metal working factory construction[RER] |
| **Output** | | | |
| Battery pack | *battery_pack* | unit | |

[a] Excludes the module electronics.

# 3. Supplementary information carbon footprint layer

Section 3.1 to 3.31 provides an overview of the different life cycle inventories used. The background database is ecoinvent 3.7.1. Transport requirement for processes located in Europe are based on the average European freight transport values as modelled in the ecoinvent 3.7.1.

## 3.1 Inventory anode active materials

Anode active materials include $SiO_x$ (maximum of 10 wt%), synthetic graphite and natural graphite. An ecoinvent process for silicon monoxide is currently not available. Metallurgy grade silicon is instead used as a proxy, similar to Philippot *et al.* (2019). Natural graphite is based on the global EI inventory market process 'graphite production, battery grade', which is a modified inventory of the original graphite production dataset by Notter et al. (2010) to include a higher energy intensity. Synthetic graphite made from pet coke and coal tar based on the GREET inventory as described by Dunn, James, et al. (2015). ecoinvent background inventories are matched to the GREET material inputs and provided in Table 3.1. The default location for synthetic production is assumed to be in China (Crenna *et al.*, 2021).

Table 3.1: Process inventory for synthetic graphite. Adoption of GREET inventory as described by Dunn *et al.* (2015) with matching ecoinvent inventories similar to Crenna *et al.* (2021)

| **Description** | **Quantity** | **Unit** | **ecoinvent process** |
|---|---|---|---|
| **Materials** | | | |
| Petroleum coke | 0.96 | kg | Market for petroleum coke [GLO] |
| Coal tar | 0.24 | kg | Market for coal tar [GLO] |
| **Processes** | | | |
| Heat | 5.43 | MJ | Market for heat, district or industrial, natural gas [RoW] |
| Electricity | 4.08 | kWh | market group for electricity, medium voltage[CN] |
| **Infrastructure** | | | |
| Facility | $7.41 \times 10^{-10}$ | unit | Market for chemical factory, organics [GLO] |
| **Transport** | | | |
| Oceanic ship | 22 | tkm | transport, freight, sea, container ship [GLO] |
| **Output** | | | |
| Synthetic graphite | 1 | kg | |

## 3.2 Inventory cathode active material (layered oxides)

Layered oxide active materials include $LiNi_xCo_yMn_zO_2$ and $LiNi_{0.8}Co_{0.15}Al_{0.05}O_2$ (hereafter NMC and NCA oxide). The production of both materials is similar and consists of two main steps: co-precipitation and calcination (Ahmed *et al.*, 2017). In the first steps, metal salts ($CoSO_4$, $NiSO_4$ and $MnSO_4$ for NMC and $NiSO_4$, $CoSO_4$ and $Al_2(SO_4)_3$ for NCA) are reacted with either sodium carbonate ($Na_2CO_3$) or hydroxide (NaOH) and ammonium hydroxide ($NH_4OH$) to produce a precursor material. In the second step, the precursor is mixed and calcinated with lithium carbonate ($Li_2CO_3$) or Li hydroxide (LiOH) in the case of NMC811 to produce the oxide.

In the literature, the most commonly used inventory for the production of NMC oxide is derived from Majeau-Bettez *et al.* (2011*a*) (Dai *et al.*, 2019*a*). However, this LCI is based on a lab scale production process (Liu *et al.*, 1999; Ngala *et al.*, 2004) which was combined with additional calculations and assumptions. Instead the updated GREET inventory for NMC materials is used here (Dai *et al.*, 2018*a*), which is based on primary data from a Chinese NMC material producer. Material inputs and quantities for NCNM 333, 622 and 811 are obtained from Dai *et al.* (2019*b*) and NMC532 from Winjobi *et al.* (2020), which is an stoichiometrically calculated inventory based on Dai *et al.* (2018*b*). Matching ecoinvent background inventories are all based on Crenna *et al.* (2021), who link the GREET inventories to ecoinvent proxies.

In the co-precipitation process, NAOH and $NH_4OH$ are added to the sulphate solution. Excess ammonia is removed from the waste water in a stripping tower and reused within the precursor production (Dai *et al.*, 2018*a*). To account for the closed-loop recycling of ammonia, only the losses of $NH_3$ after the stripping process are accounted (10% loss and 0.486 kg $NH_3$ required per kg of $NH_4OH$) for based on Crenna *et al.* (2021). The co-precipitation and calcination process takes place in two different facilities (Dai *et al.*, 2018*a*), and modelled as two separate inventories. Transport between the two facilities is not accounted for. The required infrastructure is based on a 27,000 ton production output and assuming a 50yr lifetime of the chemical factory. All input requirements for the precursor production of all NMC types are the same with the exception of the Ni, Co, and Mn sulphates as highlighted in table 3.2. In addition, LiOH is used for NMC811 instead of $Li_2CO_3$ in the oxide production step.

Table 3.2: Process inventory for NMC333/532/622/811 precursor production

| Description | Quantity | Unit | ecoinvent process |
|---|---|---|---|
| **Materials** | | | |
| $NiSO_4$ | 0.56/0.87/ 1.01/1.34 | kg | Market for nickel sulfate [GLO] |
| $CoSO_4$ | 0.56/0.35/ 0.34/0.17 | kg | See Section 3.5 |
| $MnSO_4$ | /0.55/0.49/ 0.33/0.16 | kg | Market for manganese sulfate [GLO] |
| $NH_4$ | $6.05 \times 10^{-3}$ | kg | Market for ammonia, anhydrous, liquid [GLO] |
| NaOH | 0.88 | kg | Market for sodium hydroxide, without water, in 50% solution state [GLO] |
| Cooling water | $6.38 \times 10^{-4}$ | $m^3$ | Water, cooling, unspecified natural origin |
| **Processes** | | | |
| Heat[a] | 40.74 | MJ | Market for heat, district or industrial, natural gas [RoW] |
| **Infrastructure** | | | |
| Facility | $7.41 \times 10^{-10}$ | unit | Market for chemical factory, organics [GLO] |
| **Output** | | | |
| Waste[b] | 1.57/1.6/ 1.56/1.52 | kg | Market for sodium sulfate, anhydrite [RoW] |
| Waste water | $6.38 \times 10^{-4}$ | $m^3$ | Wastewater average |
| Ammonia | $6.05 \times 10^{-2}$ | kg | Ammonia, to air |
| Waste water | $6 \times 10^{-4}$ | $m^3$ | Market for wastewater, average |
| NMC333/532/622 | 1 | kg | |

[a] 38.618 mmBTU/tonne of NMC precursor

[b] Waste sodium sulfate, mass balance based on Crenna *et al.* (2021).

Table 3.3: Process inventory for NMC333/532/622/811 active material production and import

| Description | Quantity | Unit | ecoinvent process |
|---|---|---|---|
| **Materials** | | | |
| LiCO | 0.38 | kg | Market for lithium carbonate [GLO] |
| LiOH[a] | 0.25 | kg | Market for lithium hydroxide [GLO] |
| NMC precursor[b] | 0.95 | kg | Table 3.2 |
| **Processes** | | | |
| Electricity | 6.87 | kWh | Market group for electricity, medium voltage [CN] |
| **Infrastructure** | | | |
| Facility | $7.4 \times 10^{-10}$ | unit | Market for chemical factory, organics [GLO] |
| **Transport** | | | |
| Oceanic ship | 22 | tkm | transport, freight, sea, container ship [GLO] |
| **Output** | | | |
| Carbon dioxide [c] | 0.21 | kg | Carbon dioxide, fossil, to air |
| Water evaporation[d] | $0.13/\ 1.96 \times 10^{-4}$ | $m^3$ | Water to air |
| Active material ($NMC_{xyz}$) | 1 | kg | |

[a] Lithium hydroxide only for NMC811.
[b] NMC333/532/622 or $811(OH)_2$ respectively.
[c] $CO_2$ emissions from thermal decomposition of LiCO. Therefore only applicable for NMC333, 532 and 622.
[d] Based on mass balance Crenna *et al.* (2021). 0.13 $m^3$ for NMC333, 532 and 622, $1.96 \times 10^{-4}$ for NMC811.

The NCA inventory is based on the GREET2 as described by Benavides *et al.* (2015) with an updated energy and water requirement as discussed in Dai *et al.* (2018*a*). Similar to NMC production, NCA is produced in two main steps. First, metal salts (Al, Co and Ni) are mixed and precipitated to obtain a NCA hydroxide ($NCA(OH)_2$) intermediate product. The molar ratio of the NCA active material is 0.80:0.15:0.05 based on Benavides *et al.* (2015) and in line with the NCA material in BatPaC. In the second process step, the $NCA(OH)_2$ is mixed with a lithium source (assuming LiOH as discused above), roasted, crushed, washed and dried to obtain the NCA active material. Similar to the NMC production inventory, it is assumed that these two produciton processes (precursor production and active material production) take place in two different facilities. Matching background ecoinvent inventories are based on (Crenna *et al.*, 2021) as well as the facility requirements and waste products (Table 3.4 and 3.5). Production takes place in China and is shipped to Europe.

Table 3.4: Process inventory for NCA precursor production

| Description | Quantity | Unit | ecoinvent process |
|---|---|---|---|
| **Materials** | | | |
| $NiSO_4$ | 1.36 | kg | Market for nickel sulfate [GLO] |
| $CoSO_4$ | 0.26 | kg | See Section 3.5 |
| $AlSO_4$ | 0.09 | kg | Market for aluminium sulfate, powder [RoW] |
| $NH_4$ | $1.81 \times 10^{-2}$ | kg | Market for ammonia, anhydrous, liquid [CN] |
| NaOH | 0.89 | kg | Market for sodium hydroxide, without water, in 50% solution state [GLO] |
| Cooling water | $6.38 \times 10^{-4}$ | $m^3$ | Water, cooling, unspecified natural origin |
| **Processes** | | | |
| Heat | 40.74 | MJ | Market for heat, district or industrial, natural gas [RoW] |
| **Infrastructure** | | | |
| Facility | $7.41 \times 10^{-10}$ | unit | Market for chemical factory, organics [GLO] |
| **Output** | | | |
| Ammonia | $1.81 \times 10^{-2}$ | kg | Ammonia, to air |
| Waster water | $6.38 \times 10^{-4}$ | $m^3$ | Market for wastewater, average |
| Waste[a] | 1.59 | kg | Market for sodium sulfate, anhydrite [RoW] |
| NCA | 1 | kg | |

[a] Waste sodium sulfate, mass balance based on Crenna *et al.* (2021).

Table 3.5: Process inventory for NCA material production and import

| Description | Quantity | Unit | ecoinvent process |
|---|---|---|---|
| **Materials** | | | |
| LiOH | 0.25 | kg | Market for lithium hydroxide [GLO] |
| NCA precursor | 0.95 | kg | Table 3.4 |
| **Processes** | | | |
| Electricity | 7.26 | kWh | Market group for electricity, medium voltage [CN] |
| **Infrastructure** | | | |
| Facility | $7.4 \times 10^{-10}$ | unit | Market for chemical factory, organics [GLO] |
| **Transport** | | | |
| Oceanic ship | 22 | tkm | transport, freight, sea, container ship [GLO] |
| **Output** | | | |
| Water evaporation | $2.4 \times 10^{-4}$/ $1.96 \times 10^{-4}$ | $m^3$ | Water to air |
| Active material (NCA) | 1 | kg | |
| Oxygen | 0.04 | kg | Oxygen, natural resource, in air |

### 3.3 Inventory spinel oxide (LMO)

Different Li Mn oxide (LMO) production routes exist which can be classified in four categories: solid state, sol-gel, hydro thermal and combustion method . Large scale production of LMO through the hydro thermal and combustion routes are challenging due the difficulty of controlling the production process and the low yields through the hydrothermal route (Susarla & Ahmed, 2020).

In the ecoinvent database, an inventory for an LMO production process based oon the solid state method is available. This dataset is based on the inventory of LMO production obtained by (Notter *et al.*, 2010) and is also used in GREET (Dunn *et al.*, 2014). Not much information about the process is available in the original publication from Notter *et al.* (2010) but the origin of this dataset is primarily based on a LMO production patent from Germany (EPA No. EP1204601) (Heil *et al.*, 2003). Here LMO is made from Mn and Li compounds, (preferably $Mn_2O_3$ and $Li_2CO_3$) through several roasting stages.

A more recent inventory, including cost and energy estimations, for LMO production is presented by Susarla & Ahmed (2020) where both the solid state and sol-gel method are presented. The solid state process inventory by (Susarla & Ahmed, 2020) is comparable to Notter *et al.* (2010) but provides more details and different assumptions , see Table 3.6. First, the Mn compound in the process by (Susarla & Ahmed, 2020) is based on electrolytic Mn dioxide (EMD) compared to an Mn oxide (Mn2O3) by (Notter *et al.*, 2010), whereby the former is more widely used as starting material (Biswal *et al.*, 2015; Lee *et al.*, 2012). Second, the process inventory by (Susarla & Ahmed, 2020) includes a significantly higher water consumption. This can be explained by the need for washing of the EMD to remove any trace amounts of metals, which also requires sulfuric acid ($H_2SO_4$). The higher amount of water requirements also translates into the higher electricity requirement for pumping power. In the process inventory by Notter *et al.* (2010), electricity is only required for the mechanical drive of the rotary kiln, resulting in a lower overall electricity demand. Finally, Susarla & Ahmed (2020) has a higher heat demand. Although the obtained values of heat demand by Notter *et al.* (2010) are not clear, the higher heat demand could be partly by the longer calcination time that is assumed.

Table 3.6: Comparison of inventories for the production of 1kg $LiMn_2O_2$.

| **Input** | **unit** | **Susarla & Ahmed (2020)[a]** | **Notter *et al.* (2010)** |
|---|---|---|---|
| $Mn_2O_3$ | kg | - | 0.918 |
| $MnO_2$ | kg | 1.017 | - |
| LiCO | kg | 0.217 | 0.215 |
| $H_2SO_4$ | kg | 0.017 | |
| Water | kg | 24.88 | 3.4 |
| Electricity | kWh | 0.079 | 0.005 |
| Heat | MJ | 22.2 | 15.3 |
| $N_2$ | kg | - | 0.786 |
| $O_2$ | kg | - | 0.715 |
| **Output** | | | |
| $CO_2$ | kg | - | 0.128 |
| LMO | kg | 1 | 1 |

[a] Inventory is based on the solid state process.

To include the LMO production process route based on EMD and the higher energy demand, the inventory by Susarla & Ahmed (2020) is used here. Most matching ecoinvent background inventories for the required materials are based on Notter *et al.* (2010) with updated values from Susarla & Ahmed (2020). For the $Mn_2O_3$, the ecoinvent for manganese dioxide production is chosen as proxy. It should be noted that this inventory is based on the chemical route of $Mn_2O_3$ production (chemical manganese dioxide (CMD)) rather than the electrochemical route (EMD). 98% of the $H_2SO_4$, used to remove any metals present in the EMD, is recovered and assumed to be reused for a second purpose off-site (Susarla & Ahmed, 2020). Non-fuel carbon dioxide emissions as a result of the LiCO+$MnO_2$ calcination are based on stoichiometric calculation (1 mol CO2 per 2 mol LMO) following a similar procedure by Dunn *et al.* (2014) for the GREET LMO inventory. Similar to the spinel oxide active materials, production is assumed to take place in China. The final inventory can be found in Table 3.7.

Table 3.7: Process inventory for LMO production

| Description | Quantity | Unit | ecoinvent process |
|---|---|---|---|
| **Materials** | | | |
| $Mn_2O_3$ | 1.02 | kg | Market for manganese dioxide[GLO] |
| LiCO | 0.217 | kg | Market for lithium carbonate [GLO] |
| $H_2SO_4$ | 0.017 | kg | Market for sulfuric acid [RoW] |
| Water | 24.88 | kg | Market for water, deionised [ROW] |
| **Processes** | | | |
| Electricity | 0.079 | kWh | Market group for electricity, medium voltage [CN] |
| Heat | 22 | MJ | Market for heat, district or industrial, natural gas [RoW] |
| **Infrastructure** | | | |
| Facility | $7.4 \times 10^{-10}$ | unit | Market for chemical factory, organics [GLO] |
| **Transport** | | | |
| Oceanic ship | 22 | tkm | transport, freight, sea, container ship [GLO] |
| **Output** | | | |
| $CO_2$ | .122 | kg | Carbon dioxide, fossil |
| $H_2SO_4$ | 0.0166 | kg | Market for sulfuric acid [RoW] |
| Active material (LMO) | 1 | kg | |

## 3.4 Inventory polyanion oxide (LFP)

LiFeP4 (LFP) active material powder production methods can be categorised in solid state and solution based methods, and several synthesis routes exist (Satyavani *et al.*, 2016). The LFP production inventory by Majeau-Bettez *et al.* (2011*b*) is adopted here as recommend by Peters & Weil (2018). This inventory is based on the solution based method (a hydro thermal process route) as described by Chen & Whittingham (2006). Here iron sulphate ($FeSO_4$) (a byproduct from the iron industry) is reacted with phosphoric acid ($H_3PO_4$) and LiOH. Similar to the spinel oxide active materials, production is assumed to take place in China. The inventory is highlighted in Table 3.8.

Table 3.8: Process inventory for LFP production

| **Description** | **Quantity** | **Unit** | **ecoinvent process** |
|---|---|---|---|
| **Materials** | | | |
| $FeSO_4$ | 1 | kg | Market for iron sulfate [RoW] |
| LiOH | 0.46 | kg | Market for lithium hydroxide [GLO] |
| $H_3PO_4$ | 0.65 | kg | Market for phosphoric acid, industrial grade [GLO] |
| Water | 46 | kg | Market for water, deionised [ROW] |
| **Processes** | | | |
| Heat | 15 | MJ | Market for heat, district or industrial, natural gas [RoW] |
| **Infrastructure** | | | |
| Facility | $7.4 \times 10^{-10}$ | unit | Market for chemical factory, organics [GLO] |
| **Transport** | | | |
| Oceanic ship | 22 | tkm | transport, freight, sea, container ship [GLO] |
| **Output** | | | |
| Iron, ion | 0.019 | kg | Iron ion, to water |
| Lithium, ion | 0.1 | kg | Lithium ion, to water |
| Waste heat | 1.5 | MJ | Heat waste, to air |
| Active material (LFP) | 1 | kg | |

## 3.5 Inventory cobalt sulphate

$CoSO_4$ production consist of three major steps, including mining, processing of ore into Co hydroxide ($Co(OH)_2$) and conversion of hydroxide into $CoSO_4$ (Dai *et al.*, 2018*b*). Currently, no ecoinvent background inventory for $CoSO_4$ is present, but an inventory for $Co(OH)_2$ based on inventory data from the Cobalt Institute does exist. The $CoSO_4$ inventory from GREET is therefore used (Dai *et al.*, 2018*b*). The matching ecoinvent background processes and quantities based on economic allocation are obtained from Crenna *et al.* (2021) who, indirectly, use this same inventory to model the production of $CoSO_4$. Similar to Dai *et al.* (2018*b*), $CoSO_4$ production is assumed to take place in China, the main $Co(OH)_2$ and $CoSO_4$ producer in the world (Baars *et al.*, 2021).

## 3.6 Inventory electrode binders, additives and solvents

Currently, a process inventory for PVDF, the cathode binder, is not present in the ecoinvent database or literature Peters & Weil (2018). The ecoinvent polyvinylfluoride (PVF) inventory is therefore used as a proxy, commonly applied in the literature (e.g. (Ellingsen *et al.*, 2016; Notter *et al.*, 2010)). N-methyl-2-pyrrolidone (NMP) is used as solvent for PVDF binders, as commonly assumed in the LCA literature. A corresponding inventory for NMP is present in ecoinvent. For the water based binder used in the anode, CMC, the ecoinvent inventory carboxymethyl cellulose, is used, similar to Peters *et al.* (2016); Crenna *et al.* (2021). No ecoinvent inventory for SBR, the CMC additive, is currently present. The SBR inventory by (Peters *et al.*, 2016) is therefore used to model the production of SBR (see Table 3.11).

Table 3.9: Process inventory of styrene-butadiene-rubber (SBR) based on (Peters *et al.*, 2016)

| **Description** | **Quantity** | **Unit** | **ecoinvent process** |
|---|---|---|---|
| **Materials** | | | |
| Butadiene | 0.72 | kg | Market for butadiene [RER] |
| Styrene | 0.25 | kg | Market for styrene [GLO] |
| Emulsifier | 0.03 | kg | Market for soap [GLO] |
| Water | 1.8 | kg | Market for water, deionised [Europe w/o CH] |
| Solvent | 0.01 | kg | Cyclohexane production [RER] |
| Initiator | $5.04 \times 10^{-3}$ | kg | Market for sodium persulfate [GLO] |
| **Processes** | | | |
| Electricity | 0.55 | kWh | Market for electricity, medium voltage [RER] |
| Heat | 13.75 | MJ | Market for heat, central or small-scale, natural gas[Europe w/o CH] |
| **Infrastructure** | | | |
| Facility | $4 \times 10^{-10}$ | unit | Market for chemical factory, organics [GLO] |
| **Transport** | | | |
| Freight train | 0.0438 | tkm | Market group for transport, freight train [RER] |
| Freight lorry | 0.1713 | tkm | Market for transport, lorry [RER] |
| Barge | 0.0219 | tkm | Market for transport, waterways, barge [RER] |
| **Output** | | | |
| NMVOC | 0.014 | kg | NMOVC, unspecified origin |
| Waste heat | 15.73 | MJ | Heat, waste, to air |
| Wastewater | 1.8 | L | wastewater, unpolluted |
| SBR | 1 | kg | |

[a] NMC/NCA, LMO and LFP electrolyte are assumed to be produced in a similar way due to the lack of data.

## 3.7 Inventory carbon black

The ecoinvent inventory 'Market for carbon black [GLO]' is used for both the anode (if present) and cathode carbon black.

## 3.8 Inventory current collectors

The inventory for the production of 1kg of anode and cathode foil material is based on Crenna *et al.* (2021). This inventory is based on the general current collector LCI as modelled in most LCA but includes a pre-treament process using sulphuric acid ($H_2SO_4$) and sodium hydroxide (NaOH) to remove impurities and guarantee resistance to corrosion. Both current collectors are assumed to be produced in Europe. The inventory for a 1 kg current collector is assumed to the same irrespective of foil thickness.

Table 3.10: Process inventory for anode current collector copper for all thicknesses

| **Description** | **Quantity** | **Unit** | **ecoinvent process** |
|---|---|---|---|
| **Materials** | | | |
| Cu | 0.72 | kg | Market copper, cathode [GLO] |
| $H_2SO_4$ | 0.205 | kg | Market for sulfuric acid [RER] |
| NaOH | 0.331 | kg | Market for sodium hydroxide, without water, in 50% solution state [GLO] |
| **Processes** | | | |
| Sheet rolling | 1 | kg | Sheet rolling, copper [RER] |
| **Infrastructure** | | | |
| Facility | $4.58 \times 10^{-10}$ | unit | Metal working factory [RER] |
| **Transport** | | | |
| Freight train | 0.0438 | tkm | Market group for transport, freight train [RER] |
| Freight lorry | 0.1713 | tkm | Market for transport, lorry [RER] |
| Barge | 0.0219 | tkm | Market for transport, waterways, barge [RER] |
| **Output** | | | |
| Waste[a] | 0.536 | kg | Market for spend solvent mixture [RER] |
| Anode current collector ($n$ µm)[b] | 1 | kg | |

[a] Waste of pretreatment ($H_2SO_4$ and NaOH) based on mass balance (Crenna *et al.*, 2021).
[b] Where $n$ refers the foil thickness including 6-12 µm

Table 3.11: Process inventory for cathode current collector aluminium for all thicknesses

| Description | Quantity | Unit | ecoinvent process |
|---|---|---|---|
| **Materials** | | | |
| Al | 0.72 | kg | Market for aluminium, wrought alloy [GLO] |
| $H_2SO_4$ | 0.205 | kg | Market for sulfuric acid [RER] |
| NaOH | 0.331 | kg | Market for sodium hydroxide, without water, in 50% solution state [GLO] |
| **Processes** | | | |
| Sheet rolling | 1 | kg | Sheet rolling, aluminium [RER] |
| **Infrastructure** | | | |
| Facility | $1.5 \times 10^{-10}$ | unit | Aluminium casting facility construction [RER] |
| **Transport** | | | |
| Freight train | 0.0438 | tkm | Market group for transport, freight train [RER] |
| Freight lorry | 0.1713 | tkm | Market for transport, lorry [RER] |
| Barge | 0.0219 | tkm | Market for transport, waterways, barge [RER] |
| **Output** | | | |
| Waste[a] | 0.536 | kg | Market for spend solvent mixture [RER] |
| Cathode current collector Al ($n$ µm)[b] | 1 | kg | |

[a] Waste of pretreatment ($H_2SO_4$ and NaOH) based on mass balance (Crenna *et al.*, 2021).
[b] Where $n$ refers the foil thickness including 10-16 µm

## 3.9 Inventory separator

All teardown report highlight the presence of a coating layer on the separator foil material such as $Al_20_3$. Coating layers on the foil materials are not commonly included in LCA despite the presence of a coated separator ecoinvent background inventory based on the study by Notter *et al.* (2010). The inclusion of a ceramic coating rather than a plain polyolefin material results in higher environmental emissions (Peters & Weil, 2018; Crenna *et al.*, 2021).

The inventory for non-coated separators is based on Ellingsen *et al.* (2014), where granulated PP is used as the input material and injection moulding as the production process (Table 3.12). The production process for the different separator thicknesses is assumed to be the same.

Table 3.12: Process inventory of non-coated PP separator based on Ellingsen *et al.* (2014)

| **Description** | **Quantity** | **Unit** | **ecoinvent process** |
|---|---|---|---|
| **Materials** | | | |
| Polypropylene | 1 | kg | Market for polypropylene, granulate [GLO] |
| **Processes** | | | |
| Production | 1 | kg | Injection moulding [RER] |
| **Infrastructure** | | | |
| Facility | $7.4 \times 10^{-10}$ | unit | Plastic processing factory construction [RER] |
| **Transport** | | | |
| Freight train | 0.0438 | tkm | Market group for transport, freight train [RER] |
| Freight lorry | 0.1713 | tkm | Market for transport, lorry [RER] |
| Barge | 0.0219 | tkm | Market for transport, waterways, barge [RER] |
| **Output** | | | |
| Separator (5/7/9 µm) [a] | 1 | kg | |

[a] Production processes for 5, 7 and 9 µm non-coated separators are assumed to be the same.

## 3.10 Inventory coated separator

The inventory of the coated separator is based on Notter *et al.* (2010) with two modification. First, the PE material (originally modelled as a PE fleece) is substituted for a PP membrane by including polypropylene as material and injection moulding as an additional process, similar to Crenna *et al.* (2021). Second, the PP:coating ratio is adjusted according to the three different separator thicknesses included in the model. The weight of the PP and coating material ($wt_{sep\_m}$) required for the production of 1 kg coated separator is calculated with Equation 3.1.

$$\boldsymbol{wt_{sep\_m} = \frac{th_{sep\_m}\rho_{sep\_m}Vsep}{th_{sep}\rho_{sep}}} \tag{3.1}$$

As discussed in Section 1, the densities ($\rho$) are 1.996 g/cm3 and 0.9 for the coating and PP layer, respectively. $\rho_{sep}$ refer to the total thickness and weight of the separator as calculated with Equation 1.5 and $th_{sep}$ to the total thickness. $V_{sep}$ refers to the porosity of the separator, which is 50% based on BatPaC.

Based on this, the inventory for coated separators is presented in Table 3.13. The quantities of PVDF (26 wt.%), hexafluorpropylene (4 wt.%),dibutyl phthalate (DBP,40 wt.%) and silica (30 wt.%) in the original inventory by Notter *et al.* (2010) are adjusted based on the weight of the coating. Process energy (heat for solvent evaporation and electricity for mechanical drive processes) and the scrap rate (5%) is assumed to remain the same.

Table 3.13: Process inventory for three different coated separators thickness types (5/7/9 µm 2/2/3µm)

| Description | Quantity | Unit | ecoinvent process |
|---|---|---|---|
| **Materials** | | | |
| Polypropylene | 0.56/0.64/0.6 | kg | Market for polypropylene, granulate [GLO] |
| Acetone | 0.014 | kg | Market for aceton, liquid [GLO] |
| Waste | 0.05 | kg | Market for residue from shredder fraction from manual dismantling [CH] |
| Hexaflouroethane | 0.02/0.01/0.02 | kg | Market for hexafluoroethane [GLO] |
| PVDF | 0.13/0.11/0.12 | kg | Market for polyvinylfluoride [GLO] (proxy for PVDF) |
| Silica | 0.15/0.12/0.13 | kg | Market for silica sand [GLO] |
| DBP | 0.2/0.16/0.18 | kg | Market for phtalic anhydride (proxy for DBP) |
| **Processes** | | | |
| Production | 0.56/0.64/0.6 | kg | Injection moulding [RER] |
| **Infrastructure** | | | |
| Facility | $4 \times 10^{-10}$ | unit | Market for chemical factory, organics [GLO] |
| **Transport** | | | |
| Freight train | 0.0438 | tkm | Market group for transport, freight train [RER] |
| Freight lorry | 0.1713 | tkm | Market for transport, lorry [RER] |
| Barge | 0.0219 | tkm | Market for transport, waterways, barge [RER] |
| **Output** | | | |
| Coated separator (5/7/9µm+2/2/3µm) | 1 | kg | |

### 3.11 Inventory electrolyte

Liquid electrolyte consists of an organic solution consisting of conducting lithium salts, carbonates as solvents and additives (Armand *et al.*, 2020*a*). Lithium hexafluorophosphate (LiPF6) as salts and ethylene carbonate (EC) and dimethyl carbonate (DMC) as solvents are most commonly used according to teardown reports and the literature (see table **??**). Small amounts of additives (¡5wt%) are used to reduce the performance (cycleability and cycle life) and safety of LiB (Zhang, 2006). The most common additive is vinylene carbonate (VC) (Kwade *et al.*, 2018; Armand *et al.*, 2020*b*).

The electrolyte is assumed to purchased by battery producers as a pre-mixed product consisting of $LiPF_6$ as Li salt, EC and DMC as solvents and VC as additive. 1.2 mole of $LiPF_6$ is assumed to be solved in EC:DMC with a ratio of 70:30 and 2% VC additive as common practise (Sun *et al.*, 2020; Majeau-Bettez *et al.*, 2011*a*; Peters & Weil, 2018; Greenwood *et al.*, 2021; Crenna *et al.*, 2021).

Different Process inventory background data proxies are used to model primary LiFP6 production (Peters & Weil, 2018). The LPF6 inventory in ecoinvent is used as is recommended by

Peters & Weil (2018). This inventory is based on Notter *et al.* (2010) and described in more detail there. Here it is assumed that the electrolyte is produced in China and transported to Europe. The rest of the inventory is primarily based on Crenna *et al.* (2021) to obtain the matching ecoinvent material, electricity and process background inventories but with a different EC:DMC ratio (30:70). The VC additive is not available in ecoinvent but modelled according to Crenna *et al.* (2021). The inventory is not repeated here.

Table 3.14: Process inventory of elecrolyte production

| Description | Quantity | Unit | ecoinvent process |
|---|---|---|---|
| **Materials** | | | |
| $LiFP_6$% | 0.126 | kg | Market for lithium hexafluorophosphate [GLO] |
| EC | 0.258 | kg | Market for ethylene carbonate [GLO] |
| DMC | 0.602 | kg | Market for dimethyl carbonate [GLO] |
| VC | 0.024 | kg | See Crenna *et al.* (2021) |
| **Processes** | | | |
| Electricity | 0.416 | kWh | Market for electricity, medium voltage [CN] |
| **Infrastructure** | | | |
| Facility | $4 \times 10^{-10}$ | unit | Market for chemical factory, organics [GLO] |
| **Transport** | | | |
| Oceanic ship | 22 | tkm | transport, freight, sea, container ship [GLO] |
| **Output** | | | |
| Electrolyte[a] | 1 | kg | |

[a] NMC/NCA, LMO and LFP electrolyte are assumed to be produced similarly due to the lack of data.

### 3.12 Inventory cell container

The inventory used for the production of 1 kg of cell container is described in Table 3.15. The ecoinvent background inventories for materials and processes is based on Crenna *et al.* (2021), who match ecoinvent inventories to the description of container production by Dai *et al.* (2019*a*) which again is based on BatPaC. The infrastructure input is based on Ellingsen *et al.* (2014), and transportation service based on European averages. The quantities of each material ($PET, Al, PP$) is determined by the battery design model.

Table 3.15: Process inventory of cell container production

| Description | Quantity/ function | Unit | ecoinvent process |
|---|---|---|---|
| **Materials** | | | |
| PET | $cell\_cont\_pet/cell\_cont$ | kg | Market for polyethylene terephthalate [GLO] |
| PP | $cell\_cont\_pp/cell\_cont$ | kg | Market for polypropylene, granulate [GLO] |
| Al | $cell\_cont\_al/cell\_cont$ | kg | Market for aluminium, wrought alloy [GLO] |
| **Processes** | | | |
| Extrusion | $cell\_cont\_pet + pp/cell\_cont$ | kg | Extrusion, plastic film [RER] |
| Sheet rolling | $cell\_cont\_al/cell\_cont$ | kg | Sheet rolling, aluminium [RER] |
| **Infrastructure** | | | |
| Facility plastics | | unit | Plastic processing factory [RER] |
| Facility Al | $7.7 \times 10^{-11}$ | unit | Aluminium casting plant [RER] |
| **Transport** | | | |
| Freight train | 0.0438 | tkm | Market group for transport, freight train [RER] |
| Freight lorry | 0.1713 | tkm | Market for transport, lorry [RER] |
| Barge | 0.0219 | tkm | Market for transport, inland waterways, barge [RER] |
| **Output** | | | |
| Cell container | 1 | kg | |

### 3.13 Inventory cell terminal

The cell terminals are made out of a thin Cu (anode) and Al (cathode) layer on both sides of the cell and cover almost the entire width of the cell (Nelson *et al.*, 2019). The required weight of each terminal is calculated in BatPaC and based on the cell geometry and thickness of the terminal material (default value is 1mm). The inventory for Al and Cu terminals are based on Ellingsen *et al.* (2014) and Crenna *et al.* (2021), assuming production takes place in Europe.

Table 3.16: Process inventory of cell terminal (cathode)

| Description | Quantity/ function | Unit | ecoinvent process |
|---|---|---|---|
| **Materials** | | | |
| Al | 1 | kg | Market for aluminium, wrought alloy [GLO] |
| **Processes** | | | |
| Sheet rolling | 1 | kg | Sheet rolling, aluminium [RER] |
| **Infrastructure** | | | |
| Facility | $1.5 \times 10^{-10}$ | unit | Aluminium casting plant [RER] |
| **Transport** | | | |
| Freight train | 0.0438 | tkm | Market group for transport, freight train [RER] |
| Freight lorry | 0.1713 | tkm | Market for transport, lorry [RER] |
| Barge | 0.0219 | tkm | Market for transport, inland waterways, barge [RER] |
| **Output** | | | |
| Cell terminal cathode | 1 | kg | |

Table 3.17: Process inventory of cell terminal (anode)

| Description | Quantity/ function | Unit | ecoinvent process |
|---|---|---|---|
| **Materials** | | | |
| Cu | 1 | kg | Market copper, cathode [GLO] |
| **Processes** | | | |
| Sheet rolling | 1 | kg | Sheet rolling, copper [RER] |
| **Infrastructure** | | | |
| Facility | $4.6 \times 10^{-10}$ | unit | Metal working factory [RER] |
| **Transport** | | | |
| Freight train | 0.0438 | tkm | Market group for transport, freight train [RER] |
| Freight lorry | 0.1713 | tkm | Market for transport, lorry [RER] |
| Barge | 0.0219 | tkm | Market for transport, inland waterways, barge [RER] |
| **Output** | | | |
| Cell terminal anode | 1 | kg | |

### 3.14 Inventory module container

The module container in BatPaC consist of a thin (default 0.3 mm) Fe sheet. Fe steel rolling is therefore used a proxy to produces this product. Similar to the battery pack jacket, a deep drawing process is also included (see Section 3.21).

Table 3.18: Process inventory of module container production for liquid cooled system

| **Description** | **Quantity/ function** | **Unit** | **ecoinvent process** |
|---|---|---|---|
| **Materials** | | | |
| Fe | 1 | kg | Market for steel, low-alloyed [GLO] |
| **Processes** | | | |
| Sheet rolling Fe | 1 | kg | Sheet rolling, steel [RER] |
| Fe shaping | 1 | kg | Deep drawing, steel, 10000 kN press, single stroke [RER] |
| **Transport** | | | |
| Freight train | 0.0438 | tkm | Market group for transport, freight train [RER] |
| Freight lorry | 0.1713 | tkm | Market for transport, lorry [RER] |
| Barge | 0.0219 | tkm | Market for transport, inland waterways, barge [RER] |
| **Output** | | | |
| Module container | 1 | kg | |

## 3.15 Inventory module terminals

The module terminal connectors in BatPaC are modelled as two 2-cm high conductors made out of 80% copper with a plastic insulation (20%). The ecoinvent background inventories are based on Crenna *et al.* (2021) for the plastic insulation and infrastructure and the Cu conductor is based on Ellingsen *et al.* (2014), with an update for the Cu material based on ecoinvent 3.7.1. Production is assumed to be in Europe and an average transportation services for Europe is included.

Table 3.19: Process inventory of module terminals

| Description | Quantity/ function | Unit | ecoinvent process |
|---|---|---|---|
| **Materials** | | | |
| Cu | 0.8 | kg | Market for copper, cathode [GLO] |
| PE | 0.2 | kg | glass fibre reinforced plastic production, polyamide, injection moulded [RER] |
| **Processes** | | | |
| Cu conductor | 0.8 | unit | Metal working, average for copper product manufacturing [RER] |
| **Infrastructure** | | | |
| Facility | 4.85E-10 | unit | Metal working factory construction [RER] |
| **Transport** | | | |
| Freight train | 0.0438 | tkm | Market group for transport, freight train [RER] |
| Freight lorry | 0.1713 | tkm | Market for transport, lorry [RER] |
| Barge | 0.0219 | tkm | Market for transport, inland waterways, barge [RER] |
| **Output** | | | |
| Module terminal | 1 | kg | |

## 3.16 Inventory module panels

The module panels consist of a

## 3.17 Inventory module thermal conductors

An aluminium heat conduction channel in the module transfers the cell heat to the cooled walls of the module (Nelson *et al.*, 2019). The weight of heat conductor is based on the cell and module geometry and determined by the specific battery design in BatPaC. The ecoinvent background inventories are based on Crenna *et al.* (2021). Production is assumed to be in Europe and an average transportation services for Europe is included.

Table 3.20: Process inventory of module thermal conductors

| Description | Quantity/ function | Unit | ecoinvent process |
|---|---|---|---|
| **Materials** | | | |
| Al | 1 | kg | Aluminium, wrought alloy [RER] |
| **Processes** | | | |
| Production | 1 | kg | Sheet rolling, aluminium [RER] |
| **Infrastructure** | | | |
| Facility | 4.85E-10 | unit | Metal working factory construction [RER] |
| **Transport** | | | |
| Freight train | 0.0438 | tkm | Market group for transport, freight train [RER] |
| Freight lorry | 0.1713 | tkm | Market for transport, lorry [RER] |
| Barge | 0.0219 | tkm | Market for transport, inland waterways, barge [RER] |
| **Output** | | | |
| Module thermal conductor | 1 | kg | |

### 3.18 Inventory polymer spacers gas release

The gas release system in the module allows for the release of excessive gas through pressure release disks at the back of the module (Nelson *et al.*, 2019). A 6mm polymer spacers are added to allow for the gas passage between the cell terminals and back of the module. The weight of the polymer spacers is calculated in BatPaC. The ecoinvent background inventories are based on Crenna *et al.* (2021). Production is assumed to be in Europe and an average transportation services for Europe is included.

Table 3.21: Process inventory of module polymer spacers gas release

| Description | Quantity/ function | Unit | ecoinvent process |
|---|---|---|---|
| **Materials** | | | |
| PE | 1 | kg | Market for polyethylene, high density, granulate [RER] |
| **Processes** | | | |
| Production | 1 | kg | Extrusion, plastic film [RER] |
| **Infrastructure** | | | |
| Facility | $7.4 \times 10^{-10}$ | unit | Plastic processing factory construction [RER] |
| **Transport** | | | |
| Freight train | 0.044 | tkm | Market group for transport, freight train [RER] |
| Freight lorry | 0.171 | tkm | Market for transport, lorry [RER] |
| Barge | 0.022 | tkm | Market for transport, inland waterways, barge [RER] |
| **Output** | | | |
| Module gas release | 1 | kg | |

## 3.19 Inventory module electronics

The electronics in the module includes a state-of-charge (SOC) regulator and cell monitoring system for malfunctions (Nelson *et al.*, 2019). The weight of the module electronics system is calculated within the BatPaC model based on user defined parameters including number of cells and number of cells in parallel. The inventory of the module electronics is based on a single ecoinvent market process for printed wiring boards based on (Ellingsen *et al.*, 2014) (referred to by the others as the battery module board): Market for printed wiring board, through-hole mounted, unspecified, Pb free [GLO].

## 3.20 Inventory cell group interconnect

If the module consists of more than one row of cells, a Cu cell group interconnect is included. The weight of the cell group interconnect is based on BatPaC. In BatPaC, the interconnect material is the same as the positive cell terminal. The inventory for the cell group interconnect is therefore the same as the negative cell terminal, see Table 3.17.

## 3.21 Inventory battery jacket

The battery pack jacket as modelled in BatPaC contains Al, Fe and insulation materials. The mass of each material is based on their respective thickness, which can be changed in BatPaC. ecoinvent background inventory for Fe, Al, sheet rolling and extrusion are based on Crenna *et al.* (2021) and Ellingsen *et al.* (2014). The material used for insulation is not disclosed in BatPaC. A polypropylene layer is instead used as a proxy based on commonly used EV battery insulation materials, as highlighted by MARIAN (2019). Crenna *et al.* (2021) suggests that the best proxy for the process of shaping battery jacket is sheet rolling and deep drawing. As a deep drawing process in ecoinvent is only available for Fe, an impact extrusion process is used for Al as suggested by Crenna *et al.* (2021).

Table 3.22: Process inventory of battery jacket

| Description | Quantity/ function | Unit | ecoinvent process |
|---|---|---|---|
| **Materials** | | | |
| Al | $pack\_cont\_al/pack\_cont$ | kg | Market for aluminium, wrought alloy [GLO] |
| Fe | $pack\_cont\_fe/pack\_cont$ | kg | Market for steel, low-alloyed [GLO] |
| Insulation (PP) | $pack\_cont\_pp/pack\_cont$ | kg | Market for polypropylene, granulate [GLO] |
| **Processes** | | | |
| Al shaping | $pack\_cont\_al/pack\_cont$ | kg | Impact extrusion of aluminium, 1 stroke [RER] |
| Sheet rolling Fe | $pack\_cont\_fe/pack\_cont$ | kg | Sheet rolling, steel [RER] |
| Fe shaping | $pack\_cont\_fe/pack\_cont$ | kg | Deep drawing, steel, 10000 kN press, single stroke [RER] |
| **Transport** | | | |
| Freight train | 0.044 | tkm | Market group for transport, freight train [RER] |
| Freight lorry | 0.171 | tkm | Market for transport, lorry [RER] |
| Barge | 0.022 | tkm | Market for transport, inland waterways, barge [RER] |
| **Output** | | | |
| Battery jacket | 1 | kg | |

### 3.22 Inventory module compression plates

The module compression plates ensure that module casings are compressed together between steel sheets to ensure intimate contact between the active layers that make up the cell that are tightly fit into the modules, and provides structural support to the module casings (Nelson *et al.*, 2019). A general steel reinforced steel and sheet rolling process is modelled based on (Ellingsen *et al.*, 2014) and (Crenna *et al.*, 2021).

Table 3.23: Process inventory for module compression plates

| Description | Quantity/ function | Unit | ecoinvent process |
|---|---|---|---|
| **Materials** | | | |
| Steel | 1 | kg | Market for reinforcing steel [GLO] |
| **Processes** | | | |
| Production | 1 | kg | Sheet rolling, steel [RER] |
| **Infrastructure** | | | |
| Facility | $4.4 \times 10^{-10}$ | unit | Metal working factory construction [RER] |
| **Transport** | | | |
| Freight train | 0.044 | tkm | Market group for transport, freight train [RER] |
| Freight lorry | 0.171 | tkm | Market for transport, lorry [RER] |
| Barge | 0.022 | tkm | Market for transport, inland waterways, barge [RER] |
| **Output** | | | |
| Module compression plates | 1 | kg | |

### 3.23 Inventory module interconnect

Modules are interconnected (negative to positive terminals) by 5cm long Cu connector (Nelson *et al.*, 2019). The Cu interconnects are modelled as a general Cu product based on Ellingsen *et al.* (2014).

Table 3.24: Process inventory for module interconnect

| Description | Quantity/ function | Unit | ecoinvent process |
|---|---|---|---|
| **Materials** | | | |
| Cu | 1 | kg | Market for copper, cathode [GLO] |
| **Processes** | | | |
| Production | 1 | kg | Copper product manufacturing, averagae metal working [RER] |
| **Infrastructure** | | | |
| Facility | $4.4 \times 10^{-10}$ | unit | Metal working factory construction [RER] |
| **Transport** | | | |
| Freight train | 0.044 | tkm | Market group for transport, freight train [RER] |
| Freight lorry | 0.171 | tkm | Market for transport, lorry [RER] |
| Barge | 0.022 | tkm | Market for transport, inland waterways, barge [RER] |
| **Output** | | | |
| Module interconnect | 1 | kg | |

### 3.24 Inventory pack terminals

In BatPaC, the pack terminals are made of 75% Cu as conductive material and 25% ceramic as insulation material. Due to the lack of ceramic inventory in ecoinvent, the insulation material is modelled as reinforced plastic based on Crenna *et al.* (2021). Copper process requirement is based on Ellingsen *et al.* (2014) and a general metal working factory used as proxy for infrastructure requirement. Production is assumed to take place in Europe.

Table 3.25: Process inventory for pack terminals

| Description | Quantity/ function | Unit | ecoinvent process |
|---|---|---|---|
| **Materials** | | | |
| Cu conductor | 0.75 | kg | Market for copper, cathode [GLO] |
| Insulation | 0.25 | kg | Glass fibre reinforced plastic production, polyamide, injection moulded[RER] |
| **Processes** | | | |
| Production | 0.75 | kg | Copper product manufacturing, average metal working [RER] |
| **Infrastructure** | | | |
| Facility | $4.4 \times 10^{-10}$ | unit | Metal working factory construction [RER] |
| **Transport** | | | |
| Freight train | 0.044 | tkm | Market group for transport, freight train [RER] |
| Freight lorry | 0.171 | tkm | Market for transport, lorry [RER] |
| Barge | 0.022 | tkm | Market for transport, inland waterways, barge [RER] |
| **Output** | | | |
| Pack terminals | 1 | kg | |

## 3.25 Inventory pack heater

When operating in cold temperatures, battery pack heaters are used to deliver full power at the vehicle startup if the temperature if less than 5°C (Nelson *et al.*, 2019). In BatPaC an electric heater is included to start-up the battery in cold temperatures. The weight of the heater is based on the power requirement (0.2 kg/kW) which differs by size of the battery and is therefore calculated in BatPaC. Pack heaters are typically not included in battery LCA and no information about the material of the pack heater is available in BatPaC. The pack heater by Crenna *et al.* (2021) based on a aluminium heating plate is therefore used as a proxy for the heating system.

Table 3.26: Process inventory for pack heater

| Description | Quantity/ function | Unit | ecoinvent process |
|---|---|---|---|
| **Materials** | | | |
| Al plate | 1 | kg | Market for aluminium, wrought alloy [GLO] |
| **Processes** | | | |
| Production | 1 | kg | Sheet rolling, aluminium [RER] |
| **Infrastructure** | | | |
| Facility | $4.58 \times 10^{-10}$ | unit | Metal working factory construction [RER] |
| **Transport** | | | |
| Freight train | 0.044 | tkm | Market group for transport, freight train [RER] |
| Freight lorry | 0.171 | tkm | Market for transport, lorry [RER] |
| Barge | 0.022 | tkm | Market for transport, inland waterways, barge [RER] |
| **Output** | | | |
| Pack heater | 1 | kg | |

### 3.26 Inventory pack busbar

A busbar is added to packs with only a single row to carry the current to the front of the pack (Nelson *et al.*, 2019). It is assumed that the busbar material is the same as the module interconnect as a single price for both components is used BatPaC. The inventory for the busbar is therefore identify to the module interconnect as described in Table 3.24.

### 3.27 Inventory coolant

In BatPaC the coolant consists of a 50/50 ethylene-glycol/deionised water (EG/W) solution, which is a low cost coolant that is commonly used in battery systems (Nelson *et al.*, 2019). General ecoinvent market processes for ethylene glycol (global) and dionised water (Europe) are used for the 50/50 coolant solution.

### 3.28 Inventory cooling tubes

The coolant tubes in BatPaC are made out of steel, and for the production of these the steel product manufacturing, average metal working is used.

Table 3.27: Process inventory for cooling tubes

| Description | Quantity/ function | Unit | ecoinvent process |
|---|---|---|---|
| **Materials** | | | |
| Steel | 1 | kg | Market for reinforcing steel [GLO] |
| **Processes** | | | |
| Production | 1 | kg | Sheet rolling, steel [RER] |
| **Infrastructure** | | | |
| Facility | $4.4 \times 10^{-10}$ | unit | Metal working factory construction [RER] |
| **Transport** | | | |
| Freight train | 0.044 | tkm | Market group for transport, freight train [RER] |
| Freight lorry | 0.171 | tkm | Market for transport, lorry [RER] |
| Barge | 0.022 | tkm | Market for transport, inland waterways, barge [RER] |
| **Output** | | | |
| Cooling tubes | 1 | kg | |

### 3.29 Inventory cooling connectors

The coolant connector material is not disclosed in BatPaC. The pipe fitting inventory by Ellingsen *et al.* (2017) is instead used as a proxy, where a mixture of rubber and polyvinylchloride material are used. The inventory is identical and not replicated here.

### 3.30 Inventory cooling panels

The cooling panels in BatPaC are made out of 0.3 mm thick Fe sheets. Fe sheet rolling is therefore used as a proxy to produce the panels. The inventory is thereby identical to the cooling tubes as highlighted in Table 3.27.

### 3.31 Inventory battery management system

Within LCA studies, different levels of detail for the battery management system (BMS) are used, whereby Ellingsen *et al.* (2014) provides the most detailed inventory (Peters & Weil, 2018). This inventory, which is based on primary data, is therefore used to model the BMS and includes the integrated battery interface system (IBIS), high voltage system, low voltage system and fasteners. The module electronic parts are excluded from the original inventory as they are already present in the module electronics inventory. Table 3.28 provides the inventory for the BMS. The LCI for the indivdiual components are not replicated here as they are identical to Ellingsen *et al.* (2014) but includes a general European transport service.

Table 3.28: Process inventory for battery management system

| **Description** | **Quantity** | **Unit** | **ecoinvent process** |
|---|---|---|---|
| **Materials** | | | |
| IBIS | 0.528 | kg | |
| IBIS fasteners | $3.0 \times 10^{-3}$ | kg | |
| High voltage system | 0.329 | kg | |
| Low voltage system | 0.142 | kg | |
| **Transport** | | | |
| Freight train | 0.044 | tkm | Market group for transport, freight train [RER] |
| Freight lorry | 0.171 | tkm | Market for transport, lorry [RER] |
| Barge | 0.022 | tkm | Market for transport, inland waterways, barge [RER] |
| **Output** | | | |
| Pack heater | 1 | kg | |

# 4. Supplementary information cost layer

## 4.1 Factor requirement and costs

Table 4.1 provides an overview of the factor requirements (labour, capital and land) for each production process of the base factor (100,000 packs per year) in BatPaC (Nelson *et al.*, 2019). These values are used to calculate the scaling vector when increasing or decreasing factory size.

Table 4.2 provides an overview of the factor cost for the considered European countries. The factor costs are multiplied by the total factor requirement to obtain the monetary factor costs. Capital is multiplied by a factor of 1.04 to convert from the 2018 dollar value used in BatPaC to 2020 dollar value. European labour cost are based on the average industry, construction and services labour costs obtained from Eurostat (2021*c*), which where previously used by both Philippot *et al.* (2019) and Duffner *et al.* (2020*a*) to estimate labour costs for a European battery cell production facility. Cost of land refers to building costs. Country specific building cost estimates are based on the two step approach by Duffner *et al.* (2020*a*). Here the detailed cost estimate for an industrial high tech factory/laboratory in the UK as reported by Townsend (2020) is used as a baseline, which are then multiplied by the percentage values of construction costs for the different countries as reported by the ECC (2021). European average in Table 4.2 refers to the average of the seven battery producing countries.

Table 4.1: Factor requirements for the battery production processes of the base factory (100,000 packs per year) in BatPaC. Values obtained from Nelson *et al.* (2019).

| | **Labour (hours year$^{-1}$)** | **Capital (million $US)** | **Land (m$^2$)** |
|---|---|---|---|
| Receiving | 24,000 | 8 | 1,600 |
| Anode mixing | 21,600 | 7 | 700 |
| Cathode mixing | 21.600 | 31 | 1,700 |
| Anode coating and drying | 36,000 | 16 | 1,200 |
| Cathode coating and drying | 50,400 | 31 | 1,700 |
| Cathode calendering | 28.800 | 2.5 | 500 |
| Anode calendering | 28.800 | 2.5 | 500 |
| Materials handling | 57,600 | 4 | 2,100 |
| Electrode slitting | 43,200 | 4 | 500 |
| Vacuum drying | 28,800 | 4 | 600 |
| Cell stacking | 72,000 | 8 | 1,800 |
| Terminal welding | 72,00 | 12 | 1,200 |
| Enclosing jelly roll | 28,800 | 4 | 600 |
| Electrolyte filling | 64,800 | 12 | 1,800 |
| Dry room management | 7,200 | 7 | 200 |
| Rack loading and formation cycling | 57,600 | 57 | 1,950 |
| Charge-retention testing | 10,800 | 4 | 1,800 |
| Cell sealing and rack unloading | 28,800 | 15 | 600 |

Table 4.2: Production factor cost in US Dollar. Labour cost obtained from Eurostat (2021*c*); capital based on conversion of 2018 dollar value to 2020 dollar value; land refers to building cost based which is calculated similar to Duffner *et al.* (2020*a*) based on data obtained from Townsend (2020) and ECC (2021).

| **Country** | **land (\$/m$^2$)** | **labour (\$/hr)** | **capital (\$/\$)** |
|---|---|---|---|
| France | 2380 | 43 | 1.04 |
| Germany | 2214 | 42 | 1.04 |
| Hungary | 1220 | 12 | 1.04 |
| Norway | 3683 | 59 | 1.04 |
| Poland | 1503 | 13 | 1.04 |
| Sweden | 3075 | 43 | 1.04 |
| Great Britain | 2291 | 34 | 1.04 |
| European average | 2338 | 35 | 1.04 |

## 4.2 Material prices - Mass

Material mass are presented in Table 4.3. Most material prices are obtained from the Shanghai Metals Market (SMM) and the BatPaC cost model. Several assumptions and additional calculates were required. First, six different battery separator types with a varying thickness and coating layer are available from the SMM. The price data for spectators was converted from m$^2$ to kg based on Equation 3.1 in Section 3.10. Second, three types of electrolyte are available from the SMMM, including NMC, LMO and LFP chemistries. It is assumed that NCA chemistries require NMC electrolytes and LMO electrolyte is only for pure LMO (i.e. LMO-NMC blends use NMC electrolyte). Third, price data for Li-NMC333, Li-NCA and Li-NMC532/LMO were not available and instead calculated. A description of this can be found in Section 4.8.

Fourth, prices for all different current collectors thicknesses included in the model are not available. While BatPaC uses a single price irrespective of the thickness, a small price difference between current collectors can be observed on the SMM. For LIB Al foils, the SMM reports a price of 2.9, 2.7 and 2.4 \$ kg$^{-1}$ for 12, 13 and 15 µm, respectively while LIB Cu foil has a price of 7.28 and 5.72 \$ kg$^{-1}$ for 6 and 8 µm (Cu foil prices refers to the treatment charges and excludes the cost of Cu raw material). To avoid the use of an average value for current collectors, the following assumption was made. For Al foil, 2.9 \$ kg$^{-1}$ was used for 10, 11 and 12 µm, 2.7 for \$ kg$^{-1}$ 13 and 14 µm and 2.4 for 15-18 µm. For Cu foil, it was assumed that 6 and 7 µm foils are sold with a treatment charges of 7.28 \$ kg$^{-1}$ while 8 - 14 µm are fixed to 5.72 \$ kg$^{-1}$. An additional cost of 9.72 kg$^{-1}$ is included to account for the current Cu price (see Table 4.5), resulting in a total Cu foil price of 17 kg$^{-1}$ for the 6 and 7 µm and 15.44 kg$^{-1}$ for the thicker types. This price is slightly higher than the 13.93 \$ kg$^{-1}$ used in BatPaC for all current collector types, which can be explained due to the currently high Cu price.

Table 4.3: Battery material prices per mass. SMM price as of 4th January 2022

| **Material** | **Price** | **Unit** | **Source** |
|---|---|---|---|

| | | | |
|---|---|---|---|
| natural graphite | 9.10 | $/kg | SMM (2022) |
| synthetic graphite | 12.16 | $/kg | SMM (2022) |
| SiO | 60.00 | $/kg | Greenwood *et al.* (2021) |
| LMO[a] | 10.98 | $/kg | SMM (2022) |
| LFP | 15.53 | $/kg | SMM (2022) |
| NCA | 39.64 | $/kg | Calculated, see appendix |
| NMC333 | 42.31 | $/kg | Calculated, see appendix |
| NMC532 | 37.97 | $/kg | SMM (2022) |
| NMC622 | 40.79 | $/kg | SMM (2022) |
| NMC811 | 42.36 | $/kg | SMM (2022) |
| NMC532/50%/LMO | 24.48 | $/kg | Calculated 50% NMC532-50%LMO |
| cathode binder (PVDF) | 9.50 | $/kg | Nelson *et al.* (2019) |
| anode binder (CMC) | 5.00 | $/kg | Greenwood *et al.* (2021) |
| anode binder additive (SBR) | 5.00 | $/kg | Greenwood *et al.* (2021) |
| carbon black | 3.60 | $/kg | Alibaba |
| binder solvent (NMP) | 2.00 | $/kg | Alibaba |
| binder solvent (deionised water) | 0.00 | $/kg | Assumed free, same as BatPaC |
| Al foil (10-12 um)[a] | 2.90 | $/kg | SMM (2022) |
| Al foil (13 &14 um)[b] | 2.75 | $/kg | SMM (2022) |
| Al foil (15-18 um)[c] | 2.43 | $/kg | SMM (2022) |
| Cu foil(6 um)[d] | 17.00 | $/kg | SMM (2022) |
| Cu foil(8-14 um)[e] | 15.43 | $/kg | SMM (2022) |
| electrolyte (NMC/NCA) | 20.06 | $/kg | SMM (2022) |
| electrolyte (LFP) | 18.65 | $/kg | SMM (2022) |
| electrolyte (LMO) | 15.05 | $/kg | SMM (2022) |
| separator (5um) | 195.56 | $/kg | SMM (2022) |
| separator (7um) | 98.41 | $/kg | SMM (2022) |
| separator (9um) | 51.85 | $/kg | SMM (2022) |
| coated separator (5um+2um) | 83.31 | $/kg | SMM (2022) |
| coated separator (7um+2um) | 51.81 | $/kg | SMM (2022) |
| coated separator (9um+3um) | 32.88 | $/kg | SMM (2022) |
| cell terminal cathode | 4.16 | $/kg | Nelson *et al.* (2019) |
| cell terminal anode | 6.24 | $/kg | Nelson *et al.* (2019) |
| cell container | 3.12 | $/kg | Nelson *et al.* (2019) |
| module container | 3.12 | $/kg | Nelson *et al.* (2019) |
| module terminal | 5.00 | $/kg | Nelson *et al.* (2019) |
| module thermal conductor | 4.00 | $/kg | Nelson *et al.* (2019) |
| cell group interconnect | 6.00 | $/kg | Nelson *et al.* (2019) |
| battery jacket | 7.00 | $/kg | Nelson *et al.* (2019) |
| module compression plates | 2.00 | $/kg | Nelson *et al.* (2019) |
| module interconnects | 5.00 | $/kg | Nelson *et al.* (2019) |

[a] Based on 12 um Al LIB foil price from SMM
[b] Based on 13 um Al LIB foil price from SMM
[c] Based on 15 um Al LIB foil price from SMM
[d] Based on a treatment charge for 6 um Cu LIB foil price from SMM and current Cu metal price
[e] Based on a treatment charge for 8 um Cu LIB foil price from SMM and current Cu metal price

## 4.3 Material prices - unit

Unit material prices are presented in Table 4.4. Unit prices refer to the additional unit price based on different pack specific parameters (unit column). All prices are based on BatPaC. The battery management system unit cost is calculated with BatPaC for each battery model pack and multiplied by 1.04 to convert from 2018 dollar value as used in BatPaC to 2020 dollar value.

Table 4.4: Battery material prices per unit based on BatPaC (Nelson *et al.*, 2019)

| **Material** | **Price (US$)** | **Unit** |
|---|---|---|
| Cell terminal cathode | 0.25 | $/cells |
| Cell terminal anode | 0.25 | $/cells |
| Module container | 1 | $/modules |
| Module terminal | 0.75 | $/modules |
| Spacer for gas release | 1.5 | $/modules |
| Module electronics | 2.5 | $/cells |
| Module electronics | 0.01 | $/module capacity |
| Cell group interconnect | 0.25 | $/interconnects |
| Module electronics | 2.5 | $/cells |
| Module thermal conductor0.1$/cells | | |
| Battery jacket | 30 | $/pack |
| Module interconnects | 1 | $/interconnect |
| Pack terminals | 15 | $/pack |
| Pack terminals | 0.03 | $/current carrying capacity |
| Busbar | 20 | $/busbar |
| Battery management system | 1.04 | $ |

[a] Calculated in BatPaC; multiplied by 1.04 to convert from 2018 BatPaC prices to 2020

## 4.4 Current mineral prices

Current mineral prices are based on a variety of sources (see Table 4.5). For Ni, Co, Mn and Li, the current (4-1-2022) prices of intermediate cathode active materials (NiSO, CoSO, MnSO and LiCO, respectively) available from the SMM are used, and adjusted to account for the elemental prices, similar to Greenwood *et al.* (2021). Al and Cu are based on 3-month contract prices obtained from the London Metal Exchange (). P and Fe are based on the phosphate rock (North Africa) and iron ore prices for December 2021 as reported by the World Bank. For Si, the current price for Si Metal Sichuan (Si¿99%) as reported by the SMM is used, similar to the monthly price monitor from the German Federal Institute for Geosciences and Natural Resources (DERA, 2021*a*). For natural graphite, the average price for 2020 of small flake graphite, the type used to make battery anode materials (USGS, 2017), as reported by Statista (2022) is used.

Table 4.5: Current mineral prices in dollar per kg of pure element

| **Mineral** | **Price (\$ $kg^{-1}$)** | **Type** | **Source** |
|---|---:|---|---|
| Ni | 24.39 | NiSO | SMM (2022) |
| Al | 2.81 | LME Al 3 months contract | LME (2022) |
| P | 1.26 | Phosphate rock, North Africa[a] | World Bank (2022) |
| Fe | 0.19 | Iron ore[b] | World Bank (2022) |
| Cu | 9.72 | LME Cu 3 months contract | LME (2022) |
| C | 0.49 | Small flake | Statista (2022) |
| Li | 225.48 | LiCO | SMM (2022) |
| Si | 3.22 | Metal Yannan, Sichuan | DERA (2021*b*) |
| Mn | 4.82 | MnSO | SMM (2022) |
| Co | 76.32 | CoSO | SMM (2022) |

[a] Based on phosphate rock price, North Africa, with 32% $P_2O_5$ content based on Moroccan phosphate rock (USGS, 2021*a*)
[b] Based on iron ore price with 62% Fe content (World Bank, 2022)

## 4.5 Historic prices.

Historic mineral prices (2000-2020) are used to obtain a minimum and maximum price as input for the price sensitivity analysis. Real dollar values (2020) and sources used for all minerals are provided in Table 4.6.

Table 4.6: Historic low and high real 2020 prices per kg of pure element

| | low | high | Type | Source |
|---|---|---|---|---|
| Ni | 7.05 | 65.13 | Cathode, LME | World Bank (2022) |
| Al | 1.46 | 3.69 | Ingot, LME | World Bank (2022) |
| P | 2.81 | 27.81 | Phosphate rock[a] | World Bank (2022) |
| Fe | 0.11 | 0.63 | Iron ore[b] | World Bank (2022) |
| Cu | 2.01 | 11.35 | >99%, LME | World Bank (2022) |
| C | 0.57 | 2.05 | Fine, -100 mesh[c] | USGS (2021*b*) |
| Li | 22.48 | 217.92[d] | LiCO | USGS (2021*b*); DERA (2021*a*) |
| Si | 1.17 | 4.30 | Si metal | USGS (2021*b*); DERA (2021*a*) |
| Mn | 3.31 | 14.60 | Mn ore | USGS (2021*b*) |
| Co | 8.90 | 114.22 | US cathodes | IMF (2022) |

[a] Based on phosphate rock price, North Africa, with 32% $P_2O_5$ content based on Moroccan phosphate rock (USGS, 2021*a*).

[b] Based on iron ore price with 62% Fe content (World Bank, 2022).

[c] The type used to make battery anode materials (USGS, 2017). Average of 95.5% carbon.

[d] Based on most recent price of LiCO as reported on the SMM.

For Cu, Ni, Al, Fe and P, prices are based on monthly prices obtained from the World Bank (2022) and the (IMF, 2022) for Co and adjusted for inflation based on the annual Consumer Price Index (OECD, 2022). A historic price overview is illustrated in Figure 4.1. Historic prices from 2000-2020 for Mn, Li, C and Si are based on annual nominal prices obtained from the annual USGS Mineral Commodity Summaries (USGS, 2021*a*). The following product types are used: Si metal, Mn ore, crystalline fine (-100 mesh, 94-97% and 90% prior to 2013) graphite flakes and LiCO. For Li prices from 2010-2020 are based on battery grade LiCO as reported by the USGS, prior to this data prices are based on average LiCO. For C, different flake size products are available (large, medium, fine) with varying prices, whereby the fine flake graphite is used to make battery anode materials (USGS, 2017). The average value of the reported range price of fine graphite is therefore used. Furthermore, average prices for Li and Si in 2021 (December 2020-November 2021) are obtained from DERA (2021*a*) and the current price from SMM (2022) to include the latest price peaks for both metals. Matching monthly price data for other minerals from this source were not available.

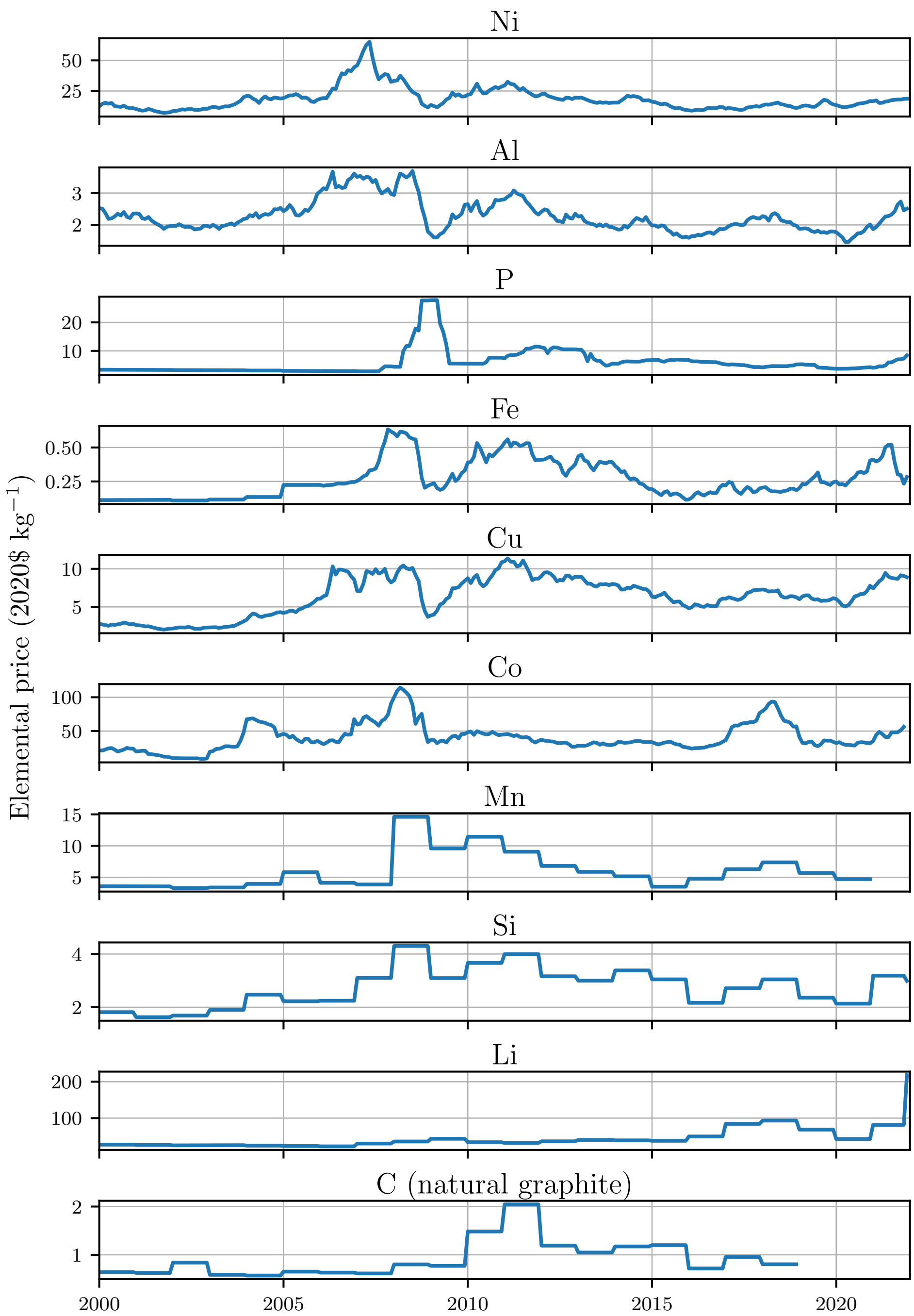


Figure 4.1: Monthly real price (2020) per kg of pure element between 2000 and 2020. Sources can be found in Table 4.6

## 4.6 Energy prices

Energy prices, including gas and electricity, for the seven considered battery producing locations are presented in Table 4.7.

Table 4.7: Electricity and gas prices for the top 7 battery producing countries in Europe. Electricity prices based on Eurostat (2021*a*) and gas based on (Eurostat, 2021*b*)

| **Country** | **Electricity ($ $kWh^{-1}$)** | **Natural gas ($ $MJ^{-1}$)** |
|---|---|---|
| FR | 0.113 | 0.012 |
| DE | 0.181 | 0.010 |
| HU | 0.110 | 0.009 |
| NO | 0.091 | 0.010 |
| PL | 0.104 | 0.011 |
| SE | 0.084 | 0.012 |
| GB | 0.176 | 0.009 |
| European average | 0.122 | 0.010 |

## 4.7 Procedure excluding energy from variable overhead cost in BatPaC

In BatPaC energy cost is included in the variable overhead cost and therefore not subject to changes in regions with lower energy prices or increasing energy consumption. The basic cost to overhead multipliers are used to estimate overhead cost as fraction of total capital, labour, land/building and material costs. Accordingly, the energy cost was deducted from the materials and purchased items multiplier based on the following calculation and procedure:

- First, the energy consumption requirement for a pack produced in the baseline plant in BatPaC was calculated based on the average electricity and natural gas consumption per kg battery, as discussed in Appendix 2.1. The pack manufactured in the baseline plant was modelled in BatPaC based on the descriptions in Nelson *et al.* (2019), including an output of 100,000 packs per year, a capacity of 60 kWh, NMC622 cathode, pack target power of 220 kW power and vehicle energy requirement of 250 Wh/mile. The modelled total cell weight (243 kg) and capacity were multiplied by the medium natural gas and electricity consumption as highlighted in Table 2.4, accounting for a 0.95 cell yield. The results indicate a total of 907.64 kWh electricity consumption and 645.46 kWh natural gas consumption per pack, or 10.76 and 15.13 kWh/kWh pack for gas and electricity respectively. Compared to the literature and the original energy consumption value of 41 kWh/kWh by Degen & Schütte (2022) this is relatively low. The main reason for this is the higher energy density of the modelled cell in the baseplant setup, 247 Wh $kg^1$ versus 123 Wh $kg^1$ used by Degen & Schütte (2022).
- Assuming the BatPaC baseplant is located in the US, average 2018[1] electricity and natural gas prices for industrial use in the US were obtained from the Energy Information Administration. For electricity this was 6.92 $ $kWh^-1$ (Eurostat, 2021*a*) and for natural gas 0.0138 $ $kWh^-1$ (EIA, 2021).[2]).
- Based on the estimated energy consumption and US price for electricity and gas, the total energy price for the BatPaC baseplant is 1.2 $ $kWh^-1$ pack, or 72$ on the pack level.

[1]BatPaC baseline plant is in 2018 prices.

[2]Based on a thousand cubic foot to therm conversion of 10.37 for natural gas.

This is a comparable value to Duffner *et al.* (2021), the only battery cost study found that states the cost of energy consumption, who states a value between 1.9 to 2.1 \$ $kWh^{-}1$ but calculates energy cost as a percentage (3%) of labour cost.

- The estimated energy cost was deducted from the basic cost to overhead multiplier. In the BatPaC baseline plant, the basic to overhead cost multiplier for materials is 1.0667, resulting in a total overhead cost related to materials of \$320 per pack. To remove the energy cost from the overhead cost multiplier, the latter was adjusted to 1.0516. Accordingly, the new overhead cost multiplier for materials was used while energy cost was estimated based on energy consumption and cost of electricity and natural gas.

## 4.8 Calculation cathode active material

Prices for NMC532-LMO, NMC333 and NCA are not available from the Shanghai Metals Market (SMM). NMC532-LMO, consisting of 50% LMO and NMC532, is calculated based on the price of LMO and NMC532, similar to LMO-$NMC_{xyz}$ blend calculation in BatPaC (Nelson *et al.*, 2019). The price for NMC333 and NCA are calculated based on the difference between intermediate metal costs and available CAM sales prices. Greenwood *et al.* (2021) refers to this difference as the product costs and profit margins (PCPM) and calculates this based on available CAM prices and intermediate material prices obtained from the Shanghai Metals Market (SMM).

To obtain the price for NMC333 and NCA, the metal cost are calculated based on the current metal prices (see also Section 4.4) and the PCPM of a comparable CAM. The PCPM for NMC333 is based on NMC532, as both are relatively mature technologies and have a comparable PCPM (Greenwood *et al.*, 2021). As pointed out by Nelson *et al.* (2012), NCA has a higher PCMP compared to low Ni NMC due to its slightly lower yield and additional raw materials required. The PCMP of NCA is therefore based on NMC622, which is slightly higher than low Ni NMC CAM (Greenwood *et al.*, 2021).

The PCPM values are also used to account for a price sensitive analysis by varying metal prices. The PCPM estimations for all cathode active materials considered are presented in Table 4.8. The differentiation in PCPM estimates between LFP, NMC532, NMC622 and NMC811 can be explained due to the differences in technology maturity and are comparable to Greenwood *et al.* (2021). Based on the current metal and CAM prices, the PCPM of LMO is negative. While the process cost of LMO is lower than other CAM due to its ease of manufacturing (Nelson *et al.*, 2012), the negative CAM price can be explained due to recent price surge of LiCO to a record high (Reuters, 2021). To account for a positive PCPM, the values of the PCPM calculation by Susarla & Ahmed (2020) are instead used in the sensitivity analysis. The authors calculate the PCPM (overheads, labour, utility costs, depreciation and profit) for LMO based on a process model for a solid-state synthesis process route utilising $MnO_2$.

Table 4.8: Cathode active material process cost and profit margin calculation (PCPM) based on current metal cost (1-2022) and cathode active material (CAM) price as reported by the SMM (2022). The PCPM price for NMC333 is based on NMC532 estimate and NCA is based on NMC622 due to lack of CAM price data.

| **Cathode** | **Unit** | **Metal cost** | **CAM price** | **Calculated PCPM** | **Used PCPM** |
|---|---|---|---|---|---|
| LFP | \$/kg | 10.23 | 15.53 | 5.30 | 5.30 |
| LMO | \$/kg | 12.64 | 10.98 | -1.66 | 3.11[a] |
| NMC333 | \$/kg | 37.24 | 42.31[b] | 5.08 | 5.08 |
| NMC532 | \$/kg | 32.89 | 37.97 | 5.08 | 5.08 |
| NMC622 | \$/kg | 33.60 | 40.79 | 7.19 | 7.19 |
| NMC811 | \$/kg | 30.90 | 42.36 | 11.46 | 11.46 |
| NCA | \$/kg | 32.45 | 39.64[c] | 7.19 | 7.19 |
| NMC532/LMO | \$/kg | 18.35 | 24.48 | 2.54 | 4.10 |

[a] Based on reported value by Ahmed *et al.* (2021).

[b] Calculated based on the current metal price and the PCPM of NMC532.

[c] Calculated based on the current metal price and the PCPM of NMC622.

# 5. Supplementary information substance flow layer

Table 5.1: Chemical elements per battery component. Values are based on reported element quantities in BatPaC or on stoichiometric calculations.

| Component | Li | Al | Si | P | Mn | Co | Ni | Cu | C |
|---|---|---|---|---|---|---|---|---|---|
| anode current collector Cu | 0.00 | 0.00 | 0.00 | 0.00 | 0.00 | 0.00 | 0.00 | 1.00 | 0.00 |
| natural graphite | 0.00 | 0.00 | 0.00 | 0.00 | 0.00 | 0.00 | 0.00 | 1.00 | 1.00 |
| battery jacket | 0.00 | 1.00 | 0.00 | 0.00 | 0.00 | 0.00 | 0.00 | 0.00 | 0.00 |
| busbar | 0.00 | 0.00 | 0.00 | 0.00 | 0.00 | 0.00 | 0.00 | 1.00 | 0.00 |
| cathode current collector Al | 0.00 | 1.00 | 0.00 | 0.00 | 0.00 | 0.00 | 0.00 | 0.00 | 0.00 |
| cell container | 0.00 | 0.82 | 0.00 | 0.00 | 0.00 | 0.00 | 0.00 | 0.00 | 0.00 |
| cell group interconnect | 0.00 | 0.00 | 0.00 | 0.00 | 0.00 | 0.00 | 0.00 | 1.00 | 0.00 |
| cell terminal anode | 0.00 | 0.00 | 0.00 | 0.00 | 0.00 | 0.00 | 0.00 | 1.00 | 0.00 |
| cell terminal cathode | 0.00 | 1.00 | 0.00 | 0.00 | 0.00 | 0.00 | 0.00 | 0.00 | 0.00 |
| electrolyte (LFP) | 0.01 | 0.00 | 0.00 | 0.00 | 0.00 | 0.00 | 0.00 | 0.00 | 0.00 |
| electrolyte (LMO) | 0.01 | 0.00 | 0.00 | 0.00 | 0.00 | 0.00 | 0.00 | 0.00 | 0.00 |
| electrolyte (NMC/NCA) | 0.01 | 0.00 | 0.00 | 0.00 | 0.00 | 0.00 | 0.00 | 0.00 | 0.00 |
| LFP | 0.04 | 0.00 | 0.00 | 0.20 | 0.00 | 0.00 | 0.00 | 0.00 | 0.00 |
| LMO | 0.04 | 0.00 | 0.00 | 0.00 | 0.59 | 0.00 | 0.00 | 0.00 | 0.00 |
| module container | 0.00 | 1.00 | 0.00 | 0.00 | 0.00 | 0.00 | 0.00 | 0.00 | 0.00 |
| module interconnects | 0.00 | 0.00 | 0.00 | 0.00 | 0.00 | 0.00 | 0.00 | 1.00 | 0.00 |
| module terminal | 0.00 | 0.00 | 0.00 | 0.00 | 0.00 | 0.00 | 0.00 | 0.80 | 0.00 |
| module thermal conductor | 0.00 | 1.00 | 0.00 | 0.00 | 0.00 | 0.00 | 0.00 | 0.00 | 0.00 |
| natural graphite | 0.00 | 0.00 | 0.00 | 0.00 | 0.00 | 0.00 | 0.00 | 0.00 | 1.00 |
| NCA | 0.07 | 0.01 | 0.00 | 0.00 | 0.00 | 0.09 | 0.49 | 0.00 | 0.00 |
| NMC333 | 0.08 | 0.00 | 0.00 | 0.00 | 0.19 | 0.20 | 0.20 | 0.00 | 0.00 |
| NMC532 | 0.08 | 0.00 | 0.00 | 0.00 | 0.17 | 0.12 | 0.30 | 0.00 | 0.00 |
| NMC532/50%/LMO | 0.04 | 0.00 | 0.00 | 0.00 | 0.38 | 0.06 | 0.15 | 0.00 | 0.00 |
| NMC622 | 0.07 | 0.00 | 0.00 | 0.00 | 0.11 | 0.12 | 0.35 | 0.00 | 0.00 |
| NMC811 | 0.04 | 0.00 | 0.00 | 0.00 | 0.06 | 0.06 | 0.47 | 0.00 | 0.00 |
| pack heater | 0.00 | 1.00 | 0.00 | 0.00 | 0.00 | 0.00 | 0.00 | 0.00 | 0.00 |
| pack terminals | 0.00 | 0.00 | 0.00 | 0.00 | 0.00 | 0.00 | 0.00 | 0.75 | 0.00 |
| SiO | 0.00 | 0.00 | 0.47 | 0.00 | 0.00 | 0.00 | 0.00 | 0.00 | 0.00 |

## Bibliography


Ahmed, S., Nelson, P., Kubal, J., Liu, Z., Knehr, K. & Dees, D. 2021 Estimated cost of ev batteries 2018-2021 - 2021 updates. `https://www.anl.gov/cse/batpac-model-software`, [Accessed January 1st, 2022].

Ahmed, S., Nelson, P. A., Gallagher, K. G., Susarla, N. & Dees, D. W. 2017 Cost and energy demand of producing nickel manganese cobalt cathode material for lithium ion batteries. *Journal of Power Sources* **342**, 733–740.

Armand, M., Axmann, P., Bresser, D., Copley, M., Edström, K., Ekberg, C., Guyomard, D., Lestriez, B., Novák, P., Petranikova, M., Porcher, W., Trabesinger, S., Wohlfahrt-Mehrens, M. & Zhang, H. 2020*a* Lithium-ion batteries – current state of the art and anticipated developments. *Journal of Power Sources* **479**, 228708.

Armand, M., Axmann, P., Bresser, D., Copley, M., Edström, K., Ekberg, C., Guyomard, D., Lestriez, B., Novák, P., Petranikova, M., Porcher, W., Trabesinger, S., Wohlfahrt-Mehrens, M. & Zhang, H. 2020*b* Lithium-ion batteries – current state of the art and anticipated developments. *Journal of Power Sources* **479**, 228708.

Baars, J., Domenech, T., Bleischwitz, R., Melin, H. E. & Heidrich, O. 2021 Circular economy strategies for electric vehicle batteries reduce reliance on raw materials. *Nature Sustainability* **4** (1), 71–79.

Benavides, P. T., Dai, Q., Sullivan, J. L., Kelly, J. C. & Dunn, J. B. 2015 Material and energy flows associated with select metals in greet 2. molybdenum, platinum, zinc, nickel, silicon. `https://greet.es.anl.gov/publication-mo-pt-zn-ni-si`, [Accessed February 3rd, 2022].

Biswal, A., Chandra Tripathy, B., Sanjay, K., Subbaiah, T. & Minakshi, M. 2015 Electrolytic manganese dioxide (emd): a perspective on worldwide production, reserves and its role in electrochemistry. *RSC Advances* **5** (72), 58255–58283.

Bryntesen, S. N., Strømman, A. H., Tolstorebrov, I., Shearing, P. R., Lamb, J. J. & Stokke Burheim, O. 2021 Opportunities for the state-of-the-art production of lib electrodes—a review. *Energies* **14** (5).

Chen, J. & Whittingham, M. S. 2006 Hydrothermal synthesis of lithium iron phosphate. *Electrochemistry Communications* **8** (5), 855–858.

Chordia, M., Nordelöf, A. & Ellingsen, L. A.-W. 2021 Environmental life cycle implications of upscaling lithium-ion battery production. *The International Journal of Life Cycle Assessment* **26** (10), 2024–2039.

Cox, B., Bauer, C., Mendoza Beltran, A., van Vuuren, D. P. & Mutel, C. L. 2020 Life cycle environmental and cost comparison of current and future passenger cars under different energy scenarios. *Applied Energy* **269**, 115021.

Crenna, E., Gauch, M., Widmer, R., Wäger, P. & Hischier, R. 2021 Towards more flexibility and transparency in life cycle inventories for lithium-ion batteries. *Resources, Conservation and Recycling* **170**, 105619.

Dai, Q., Dunn, J. B., Kelly, J. C. & Elgowainy, A. 2017 Update of life cycle analysis of lithium-ion batteries in the greet model. https://greet.es.anl.gov/publication-Li$_battery_update_2017$, [$AccessedJanuary1st$, 2022].

Dai, Q., Kelly, J. C., Dunn, J. B. & Benavides, P. T. 2018*a* Update of bill-of-materials and cathode materials production for lithium-ion batteries in the greet model. `https://greet.es.anl.gov/publication-update_bom_cm`, [Accessed December 19, 2021].

Dai, Q., Kelly, J. C. & Elgowainy, A. 2018*b* Cobalt life cycle analysis update for the greet mode. `https://greet.es.anl.gov/publication-update_cobalt`, [Accessed December 19, 2021].

Dai, Q., Kelly, J. C., Gaines, L. & Wang, M. 2019*a* Life cycle analysis of lithium-ion batteries for automotive applications. *Batteries* **5** (2), 48.

Dai, Q., Spangenberger, J., Ahmed, S., Gaines, L., Kelly, J. C. & Wang, M. 2019*b* Everbatt: A closed-loop battery recycling cost and environmental impacts model. Report. Argonne National Lab.(ANL), Argonne, IL (United States).

Davidsson Kurland, S. 2019 Energy use for gwh-scale lithium-ion battery production. *Environmental Research Communications* **2** (1), 012001.

Degen, F. & Schütte, M. 2022 Life cycle assessment of the energy consumption and ghg emissions of state-of-the-art automotive battery cell production. *Journal of Cleaner Production* **330**, 129798.

Deng, Y., Li, J., Li, T., Gao, X. & Yuan, C. 2017 Life cycle assessment of lithium sulfur battery for electric vehicles. *Journal of Power Sources* **343**, 284–295.

DERA 2021*a* Preismonitor november 2021. `https://www.deutsche-rohstoffagentur.de/DERA/DE/Produkte/Rohstoffpreise/Preismonitor/preismonitor_node.html`, [Accessed January 4th, 2022].

DERA 2021*b* Volatilitätsmonitor november 2021. `https://www.bgr.bund.de/EN/Themen/Min_rohstoffe/Produkte/produkte_node_en.html?tab=Commodity+prices`, [Accessed January 1st, 2022].

Duffner, F., Krätzig, O. & Leker, J. 2020*a* Battery plant location considering the balance between knowledge and cost: A comparative study of the eu-28 countries. *Journal of Cleaner Production* **264**, 121428.

Duffner, F., Mauler, L., Wentker, M., Leker, J. & Winter, M. 2021 Large-scale automotive battery cell manufacturing: Analyzing strategic and operational effects on manufacturing costs. *International Journal of Production Economics* **232**, 107982.

Duffner, F., Wentker, M., Greenwood, M. & Leker, J. 2020*b* Battery cost modeling: A review and directions for future research. *Renewable and Sustainable Energy Reviews* **127**, 109872.

Dunn, J. B., Gaines, L., Barnes, M., Sullivan, J. L. & Wang, M. 2014 Material and energy flows in the materials production, assembly, and end-of-life stages of the automotive lithium-ion battery life cycle. https://greet.es.anl.gov/publication-li-ion, [Accessed January 1st, 2022].

Dunn, J. B., James, C., Gaines, L., Gallagher, K., Dai, Q. & Kelly, J. C. 2015 Material and energy flows in the production of cathode and anode materials for lithium ion batteries. https://greet.es.anl.gov/publication-anode-cathode-liion, [Accessed January 1st, 2022].

ECC 2021 European construction costs: cost index. http://constructioncosts.eu/cost-index/, [Accessed January 1st, 2022].

EIA, U. 2021 Natural gas industrial prices. https://www.eia.gov/dnav/ng/NG_PRI_SUM_A_EPG0_PIN_DMCF_A.htm, [Accessed January 1st, 2022].

Ellingsen, L. A.-W., Hung, C. R. & Strømman, A. H. 2017 Identifying key assumptions and differences in life cycle assessment studies of lithium-ion traction batteries with focus on greenhouse gas emissions. *Transportation Research Part D: Transport and Environment* **55**, 82–90.

Ellingsen, L. A.-W., Majeau-Bettez, G., Singh, B., Srivastava, A. K., Valøen, L. O. & Strømman, A. H. 2014 Life cycle assessment of a lithium-ion battery vehicle pack. *Journal of Industrial Ecology* **18** (1), 113–124.

Ellingsen, L. A.-W., Singh, B. & Strømman, A. H. 2016 The size and range effect: lifecycle greenhouse gas emissions of electric vehicles. *Environmental Research Letters* **11** (5), 054010.

EPA 2021*a* Data on cars used for testing fuel economy. https://www.epa.gov/compliance-and-fuel-economy-data/data-cars-used-testing-fuel-economy, [Accessed January 1st, 2022].

EPA 2021*b* EPA's transportation and air quality document index system (dis). https://iaspub.epa.gov/otaqpub/, [Accessed January 1st, 2022].

Eurostat 2021*a* Electricity prices for non-household consumers - NRG_PC_205. https://ec.europa.eu/eurostat/databrowser/view/nrg_pc_205/default/table?lang=en, [Accessed January 1st, 2022].

Eurostat 2021*b* Gas prices for non-household consumers - NRG_PC_203. https://ec.europa.eu/eurostat/databrowser/view/nrg_pc_203/default/table?lang=en, [Accessed January 1st, 2022].

EUROSTAT 2021*c* Labour cost levels by NACE Rev. 2 activity (lc_lci_lev). `https://ec.europa.eu/eurostat/databrowser/view/lc_lci_lev/default/table?lang=en`, [Accessed January 2nd, 2022].

EV-DATABASE 2021 All electric vehicles. `https://ev-database.org`, [Accessed January 1st, 2022].

GALLAGHER, K. G. & NELSON, P. A. 2014 Manufacturing costs of batteries for electric vehicles. In *Lithium-Ion Batteries*, pp. 97–126.

GREENWOOD, M., WENTKER, M. & LEKER, J. 2021 A bottom-up performance and cost assessment of lithium-ion battery pouch cells utilizing nickel-rich cathode active materials and silicon-graphite composite anodes. *Journal of Power Sources Advances* **9**, 100055.

HEIL, G., KORMANN, C. & ADEL, J. 2003 Lithium oxide containing lithium intercalation compounds. *European Patent Application No. EP1204601, published on* **2**, 19.

IMF 2022 Primary commodity price system. `https://www.imf.org/en/Research/commodity-prices`, [Accessed January 4th, 2022].

JINASENA, A., BURHEIM, O. S. & STRØMMAN, A. H. 2021 A flexible model for benchmarking the energy usage of automotive lithium-ion battery cell manufacturing. *Batteries* **7** (1), 14.

KALLITSIS, E., KORRE, A., KELSALL, G., KUPFERSBERGER, M. & NIE, Z. 2020 Environmental life cycle assessment of the production in china of lithium-ion batteries with nickel-cobalt-manganese cathodes utilising novel electrode chemistries. *Journal of Cleaner Production* **254**, 120067.

KIM, H. C. & WALLINGTON, T. J. 2016 Life cycle assessment of vehicle lightweighting: A physics-based model to estimate use-phase fuel consumption of electrified vehicles. *Environ Sci Technol* **50** (20), 11226–11233.

KIM, H. C., WALLINGTON, T. J., ARSENAULT, R., BAE, C., AHN, S. & LEE, J. 2016 Cradle-to-gate emissions from a commercial electric vehicle li-ion battery: A comparative analysis. *Environ Sci Technol* **50** (14), 7715–22.

KWADE, A., HASELRIEDER, W., LEITHOFF, R., MODLINGER, A., DIETRICH, F. & DROEDER, K. 2018 Current status and challenges for automotive battery production technologies. *Nature Energy* **3** (4), 290–300.

LAIN, M. J., BRANDON, J. & KENDRICK, E. 2019 Design strategies for high power vs. high energy lithium ion cells. *Batteries* **5** (4), 64.

LEE, J.-W., KIM, J.-I. & ROH, K. C. 2012 Lithium manganese oxide with excellent electrochemical performance prepared from chemical manganese dioxide for lithium ion batteries. *Solid State Sciences* **14** (9), 1251–1255.

LIU, Z., YU, A. & LEE, J. Y. 1999 Synthesis and characterization of lini1xycoxmnyo2 as the cathode materials of secondary lithium batteries. *Journal of Power Sources* **81-82**, 416–419.

LME 2022 Reports by metal. `https://www.lme.com/Market-Data/Reports-and-data/Reports-by-metal`, [Accessed January 4th, 2022].

Majeau-Bettez, G., Hawkins, T. R. & Stromman, A. H. 2011*a* Life cycle environmental assessment of lithium-ion and nickel metal hydride batteries for plug-in hybrid and battery electric vehicles. *Environ Sci Technol* **45** (10), 4548–54.

Majeau-Bettez, G., Stromman, A. H. & Hertwich, E. G. 2011*b* Evaluation of process- and input-output-based life cycle inventory data with regard to truncation and aggregation issues. *Environ Sci Technol* **45** (23), 10170–7.

MARIAN 2019 Four insulating materials for use in ev batteries. `https://blog.marianinc.com/blog/4-insulating-materials-for-use-in-ev-batery`, [Accessed January 1st, 2022].

Nelson, P., Gallagher, K., Bloom, I. & Dees, D. 2012 Modeling the performance and cost of lithium-ion batteries for electric-drive vehicles - second edition. `https://www.osti.gov/biblio/1209682-modeling-performance-cost-lithium-ion-batteries-electric-drive-vehicles-second-edition`, [Accessed January 4th, 2022].

Nelson, P., Gallagher, K., Bloom, I. & Dees, D. 2019 Modeling the performance and cost of lithium-ion batteries for electric-drive vehicles - third edition. `https://publications.anl.gov/anlpubs/2011/10/71302.pdf`, [Accessed January 1st, 2022].

Ngala, J. K., Chernova, N. A., Ma, M., Mamak, M., Zavalij, P. Y. & Whittingham, M. S. 2004 The synthesis, characterization and electrochemical behavior of the layered lini0.4mn0.4co0.2o2 compound. *Journal of Materials Chemistry* **14** (2), 214–220.

Notter, D. A., Gauch, M., Widmer, R., Wäger, P., Stamp, A., Zah, R. & Althaus, H.-J. 2010 Contribution of li-ion batteries to the environmental impact of electric vehicles. *Environmental Science & Technology* **44** (17), 6550–6556.

OECD 2022 Inflation (cpi). `https://data.oecd.org/price/inflation-cpi.htm`, [Accessed January 4th, 2022].

Peters, J., Buchholz, D., Passerini, S. & Weil, M. 2016 Life cycle assessment of sodium-ion batteries. *Energy  Environmental Science* **9** (5), 1744–1751.

Peters, J. F., Baumann, M., Zimmermann, B., Braun, J. & Weil, M. 2017 The environmental impact of li-ion batteries and the role of key parameters – a review. *Renewable and Sustainable Energy Reviews* **67**, 491–506.

Peters, J. F. & Weil, M. 2018 Providing a common base for life cycle assessments of li-ion batteries. *Journal of Cleaner Production* **171**, 704–713.

Pettinger, K.-H. & Dong, W. 2016 When does the operation of a battery become environmentally positive? *Journal of The Electrochemical Society* **164** (1), A6274–A6277.

Pettinger, K.-H., Kampker, A., Hohenthanner, C.-R., Deutskens, C., Heimes, H. & vom Hemdt, A. 2018 Lithium-ion cell and battery production processes. In *Lithium-Ion Batteries: Basics and Applications* (ed. R. Korthauer), pp. 211–226. Berlin, Heidelberg: Springer.

Philippot, M., Alvarez, G., Ayerbe, E., Van Mierlo, J. & Messagie, M. 2019 Eco-efficiency of a lithium-ion battery for electric vehicles: Influence of manufacturing country and commodity prices on ghg emissions and costs. *Batteries* **5** (1), 23.

Quinn, J. B., Waldmann, T., Richter, K., Kasper, M. & Wohlfahrt-Mehrens, M. 2018 Energy density of cylindrical li-ion cells: A comparison of commercial 18650 to the 21700 cells. *Journal of The Electrochemical Society* **165** (14), A3284–A3291.

Reuters 2021 Lithium price surge could charge demand for lead in batteries. `https://www.reuters.com/markets/commodities/lithium-price-surge-could-charge-demand-lead-batteries-2021-12-16/`, [Accessed January 1st, 2022].

Safoutin, M., McDonald, J. & Ellies, B. 2018 Predicting the future manufacturing cost of batteries for plug-in vehicles for the u.s. environmental protection agency (epa) 2017–2025 light-duty greenhouse gas standards. *World Electric Vehicle Journal* **9** (3), 42.

Sankaran, G. & Venkatesan, S. 2021 Standardization of electric vehicle battery pack geometry form factors for passenger car segments in india. *Journal of Power Sources* **502**, 230008.

Satyavani, T. V. S. L., Srinivas Kumar, A. & Subba Rao, P. S. V. 2016 Methods of synthesis and performance improvement of lithium iron phosphate for high rate li-ion batteries: A review. *Engineering Science and Technology, an International Journal* **19** (1), 178–188.

Sieg, J., Bandlow, J., Mitsch, T., Dragicevic, D., Materna, T., Spier, B., Witzenhausen, H., Ecker, M. & Sauer, D. U. 2019 Fast charging of an electric vehicle lithium-ion battery at the limit of the lithium deposition process. *Journal of Power Sources* **427**, 260–270.

SMM 2022 Shanghai metals market - new energy. `https://www.metal.com/`, [Accessed January 4th, 2022].

Statista 2022 Graphite prices worldwide from 2011 to 2020, by flake grade. `https://www.statista.com/statistics/452304/graphite-prices-worldwide-prediction-by-flake-grade/`, [Accessed January 1st, 2022].

Sun, X., Luo, X., Zhang, Z., Meng, F. & Yang, J. 2020 Life cycle assessment of lithium nickel cobalt manganese oxide (NCM) batteries for electric passenger vehicles. *Journal of Cleaner Production* **273**, 123006.

Susarla, N. & Ahmed, S. 2020 Estimating the cost and energy demand of producing lithium manganese oxide for li-ion batteries. Report. Argonne National Lab.(ANL), Argonne, IL (United States).

Townsend, T. . 2020 International construction market survey. https://www.turnerandtownsend.com/en/perspectives/international-construction-market-survey-2019/, [Accessed January 1st, 2022].

USGS 2017 Graphite [advance release]. In *Minerals Yearbook* (ed. USGS), pp. 32.1 – 32.14. Reston: U.S. Geological Survey.

USGS 2021*a* Mineral commodity summaries. https://www.usgs.gov/centers/national-minerals-information-center/mineral-commodity-summaries, [Accessed January 4th, 2022].

USGS 2021*b* Minerals yearbook [tables only]. https://www.usgs.gov/centers/national-minerals-information-center/manganese-statistics-and-information, [Accessed January 4th, 2022].

Vaalma, C., Buchholz, D., Weil, M. & Passerini, S. 2018 A cost and resource analysis of sodium-ion batteries. *Nature Reviews Materials* **3**, 18013.

Wang, F., Deng, Y. & Yuan, C. 2020 Life cycle assessment of lithium oxygen battery for electric vehicles. *Journal of Cleaner Production* **264**, 121339.

Warner, J. 2015 Basic terminology. In *The Handbook of Lithium-Ion Battery Pack Design*, pp. 23–33. Cham: Elsevier.

Winjobi, O., Dai, Q. & Kelly, J. C. 2020 Update of bill-of-materials and cathode chemistry addition for lithium-ion batteries in greet 2020. https://greet.es.anl.gov/publication-li_update_2020, [Accessed January 1st, 2022].

World Bank 2022 World bank commodity price data - annual prices, 1960 to present, real 2010 us dollars. https://www.worldbank.org/en/research/commodity-markets, [Accessed January 4th, 2022].

Yuan, C., Deng, Y., Li, T. & Yang, F. 2017 Manufacturing energy analysis of lithium ion battery pack for electric vehicles. *CIRP Annals* **66** (1), 53–56.

Zhang, S. S. 2006 A review on electrolyte additives for lithium-ion batteries. *Journal of Power Sources* **162** (2), 1379–1394.